

System Size and Energy Dependence of Dilepton Production in Heavy-Ion Collisions at SIS Energies

E.L. Bratkovskaya,^{1,2} J. Aichelin,³ M. Thome,³ S. Vogel,¹ and M. Bleicher^{1,2}

¹*Institute for Theoretical Physics, Frankfurt University, 60438 Frankfurt-am-Main, Germany*

²*Frankfurt Institut for Advanced Studies, Frankfurt University, 60438 Frankfurt-am-Main, Germany*

³*SUBATECH, Laboratoire de Physique Subatomique et des Technologies Associées,
Université de Nantes - IN2P3/CNRS - Ecole des Mines de Nantes
4 rue Alfred Kastler, F-44072 Nantes, Cedex 03, France*

We study the dilepton production in heavy-ion collisions at energies of 1-2 $AGeV$ as well as in proton induced pp, pn, pd and $p + A$ reactions from 1 GeV up to 3.5 GeV where data have been taken by the HADES collaboration. For the analysis we employ three different transport models - the microscopic off-shell Hadron-String-Dynamics (HSD) transport approach, the Isospin Quantum Molecular Dynamics (IQMD) approach as well as the Ultra-relativistic Quantum Molecular Dynamics (UrQMD) approach. We find that the HSD and IQMD models provide a good description of the presently available experimental data and agree with each other reasonably well. This allows to obtain model independent conclusions on the underlying physical phenomena. In particular, we confirm the experimentally observed enhancement of the dilepton yield (normalized to the multiplicity of neutral pions N_{π^0}) in heavy-ion collisions with respect to that measured in $NN = (pp + pn)/2$ collisions. We identify two contributions to this enhancement: a) the pN bremsstrahlung which scales with the number of collisions and not with the number of participants, i.e. pions; b) the dilepton emission from intermediate Δ 's which are part of the reaction cycles $\Delta \rightarrow \pi N; \pi N \rightarrow \Delta$ and $NN \rightarrow N\Delta; N\Delta \rightarrow NN$. With increasing system size more generations of intermediate Δ 's are created. If such Δ decays into a pion, the pion can be reabsorbed, however, if it decays into a dilepton, the dilepton escapes from the system. Thus, experimentally one observes only one pion (from the last produced Δ) whereas the dilepton yield accumulates the contributions from all Δ 's of the cycle. We show as well that the Fermi motion enhances the production of pions and dileptons in the same way. Furthermore, employing the off-shell HSD approach, we explore the influence of in-medium effects like the modification of self-energies and spectral functions of the vector mesons due to their interactions with the hadronic environment. We find only a modest influence of the in-medium effects on the dilepton spectra in the invariant mass range where data with small error bars exist.

PACS numbers: 25.75.-q, 25.40.-h

I. INTRODUCTION

According to the theory of strong interactions, the Quantum Chromo Dynamics (QCD), hadrons are bound objects of quarks and gluons. The properties of hadrons in vacuum are well known and confirmed by lattice QCD calculations [1] while the properties of hadrons in a strongly interacting environment are subject of intensive research. QCD inspired approaches as well as phenomenological models based on phase shifts and $SU(3)$ symmetry [1–14] predict significant changes of hadron properties in a strongly interacting medium. The results of the different models vary substantially. It is therefore one of the challenges of novel experimental heavy-ion physics to study these in-medium modifications of hadrons. Besides the in-medium properties of the antikaon, interesting also for astrophysical reasons, the vector mesons and especially the ρ meson have been in the focus of the theoretical interest because the ρ has the quantum numbers of a photon and can therefore disintegrate into an electron-positron pair. Having only electromagnetic interactions this pair may easily leave the reaction region without further collisions. This allows to reconstruct the invariant mass of the decaying ρ^0 . Thus there is a hope that by measuring the dilepton invariant mass spectra the in-medium mass and width of the ρ meson become experimentally accessible. For this it is necessary to separate the background from known dilepton sources – Dalitz decays of baryonic and mesonic resonances as well as pN and πN bremsstrahlung. At SPS energies of 40 and 158 $AGeV$ such an enhancement above the known background has been measured by the CERES [15] and the NA60 [16] collaborations. The experimental results are compatible with the assumption that in the medium the peak position of the ρ meson mass distribution remains rather unchanged while the width increases considerably (cf. [17–22]).

At much lower energies, at energies around 1 $AGeV$ dileptons have been measured in heavy-ion collisions at the BEVALAC in Berkeley by the DLS Collaboration [23–26]. These data led to the so called 'DLS puzzle' because the DLS dilepton yield in $C + C$ and $Ca + Ca$ collisions in the invariant mass range from 0.2 to 0.5 GeV [26] was about five times higher than the results from different transport models at that time using the 'conventional' dilepton sources such as bremsstrahlung, π^0, η, ω and Δ Dalitz decays and direct decay of vector mesons (ρ, ω, ϕ) [27–29]. This discrepancy

remained even after including in the transport calculations the different scenarios for the in-medium modifications of vector meson properties, as dropping mass or collisional broadening of the ρ and ω spectral functions [30–33]. To solve this puzzle was one of the main motivations to build the HADES (High Acceptance Dilepton Spectrometer) detector at GSI in Germany [34, 34–39]. In 2008 the HADES collaboration confirmed the DLS data [34, 35] for $C + C$ at 1.0 $AGeV$. In the mean time also the theoretical transport approaches as well as effective models for the elementary NN reactions have been further developed. As it has been suggested in Ref. [40], the DLS puzzle can be solved when incorporating stronger pn and pp bremsstrahlung contributions in line with the updated One-Boson-Exchange (OBE) model calculations from [41]. The previous OBE approaches [42] used in the old transport calculations for the analysis of the DLS data, gave results close to the soft photon approximation. As shown in Ref. [40] the results of the HSD model (off-shell microscopic Hadron-String-Dynamics (HSD) transport approach) with ‘enhanced’ bremsstrahlung cross sections agree very well with the HADES experimental data for $C + C$ at 1 and 2 $AGeV$ as well as with the DLS data for $C + C$ and $Ca + Ca$ at 1 $AGeV$, especially when one includes a collisional broadening in the vector-meson spectral functions. Similar results have been obtained by other, independent transport approaches – IQMD [45] and the Rossendorf BUU [46].

Despite of the fact that theory predicts that the vector meson properties are modified substantially already at energies as low as 1-2 $AGeV$, it is quite difficult to observe these changes experimentally. The production yield of ρ^0 and ω mesons is small at these energies and the background from other dilepton sources like Δ -Dalitz decay and pn bremsstrahlung is large in the mass range of interest, $M > 0.4 GeV$. Therefore the presently available data do not allow for a detailed investigation of the in-medium properties of vector mesons.

This focuses the interest of the present studies to the question whether the invariant mass spectrum below the ρ/ω peak depends on the system size and on the beam energy in a non-trivial way, i.e. whether the dilepton invariant mass spectra can be understood as a superposition of individual pp and pn interactions. In a first publication [37] the HADES collaboration found that the invariant mass spectra of dileptons, observed in 1 and 2 $AGeV C + C$ collisions, are practically coincident below $M = 0.4 GeV$ if divided by the total number of observed π^0 and after subtracting the η Dalitz decay contribution. It is strongly suppressed at 1 $AGeV$ but becomes essential at 2 $AGeV$ due to the kinematical threshold for the η production in NN collisions. This scaling with the π^0 number can be interpreted as a scaling with the number of participants N_{part} . The HADES collaboration, comparing the dilepton yield from the light $C + C$ systems with the elementary pp and pn interactions, albeit taken at different energies, has concluded that the dilepton invariant mass spectra in these light systems can be considered as a mere superposition of pn and pp collisions without any ‘in-medium’ enhancement.

In a more recent publication [39] a heavier system, $Ar + KCl$ at 1.75 $AGeV$, was investigated and the collaboration came to the conclusion that in this reaction the dilepton invariant mass yield between 0.2 and 0.6 GeV is about 2-3 times larger than expected from a mere superposition of pp and pn collisions [39]. It is not obvious why dilepton production in this mass range does not scale with the number of pions which is proportional to the number of participants, N_{part} . From the analysis of the excess in the transverse-mass slope and from the angular anisotropies the HADES collaboration concluded that the excess of dileptons in the low invariant mass region scales with the system size very differently than the freeze-out yield of pions and η and that the data are compatible with the assumption that they originate from Δ Dalitz decays, being suggestive of resonance matter [39].

It is the purpose of the present study to investigate this enhancement within the presently available transport codes – HSD, IQMD and UrQMD – in order to explore whether the dilepton production in these systems can be reproduced by the theoretical approaches and to identify eventually the origin of this in-medium enhancement. All these codes have been successfully employed to investigate a multitude of experimental observables. They are, however, not of the same sophistication as far as the dileptons are concerned. The dilepton part of the UrQMD program is still under development and up to now bremsstrahlung is not included. This limits the predictive power to parts of the spectra where bremsstrahlung is not essential. For the study of the in-medium enhancement we limit ourselves to HSD and IQMD calculations. We start out in section II with a short description of the HSD model and of the improvements made compared to the ‘standard’ HSD 2.5 version used for the extended dilepton study in Ref. [40]. Then we come to a brief description of dilepton production in IQMD. In section III the dilepton production in elementary reactions, measured by the HADES and and DLS collaboration, is compared with HSD and IQMD calculations. The fourth section is devoted to the study of dilepton production in heavy-ion collisions. We discuss our calculations for all systems which have been measured by the HADES collaboration and present also our predictions for $Au + Au$ collision at 1.25 $AGeV$ which is presently analysed. After checking that the invariant mass spectra of dileptons in heavy-ion collisions are well reproduced by the HSD as well as by the IQMD approach we study in section V the enhancement of the dilepton production in heavy-ion collisions as compared to the elementary reactions and identify its origin. In section VI we present our conclusions.

II. THE TRANSPORT MODELS

A. The HSD model

Our analysis of the experimental results is carried out within the off-shell HSD transport model [40, 47–49] - based on covariant self energies for the baryons [50]. It has been used for the description of pA and AA collisions from SIS to RHIC energies. We recall that in the HSD approach nucleons, Δ 's, $N^*(1440)$, $N^*(1535)$, Λ , Σ and Σ^* hyperons, Ξ 's, Ξ^* 's and Ω 's as well as their antiparticles are included on the baryonic side whereas the 0^- and 1^- octet states are incorporated in the mesonic sector. Inelastic baryon–baryon (and meson-baryon) collisions with energies above $\sqrt{s_{th}} \simeq 2.6$ GeV (and $\sqrt{s_{th}} \simeq 2.3$ GeV) are described by the FRITIOF string model [51] whereas low energy hadron–hadron collisions are modelled using experimental cross sections.

The dilepton production by the decay of a (baryonic or mesonic) resonance R can be schematically presented in the following way:

$$BB \rightarrow RX \tag{1}$$

$$mB \rightarrow RX \tag{2}$$

$$R \rightarrow e^+e^-X, \tag{3}$$

$$R \rightarrow mX, m \rightarrow e^+e^-X, \tag{4}$$

$$R \rightarrow R'X, R' \rightarrow e^+e^-X. \tag{5}$$

In a first step a resonance R might be produced in baryon-baryon (BB) or meson-baryon (mB) collisions (1), (2). Then this resonance can either couple directly to dileptons (3) (e.g. Dalitz decay of the Δ resonance: $\Delta \rightarrow e^+e^-N$) or produces mesonic (4) or baryonic (5) resonances which then produce dileptons via direct decays (ρ, ω) or Dalitz decays (π^0, η, ω). With increasing energy hadrons are created by non-resonant mechanisms or string decay. This is also true for those which disintegrate into dileptons. The electromagnetic part of all conventional dilepton sources – $\pi^0, \eta, \omega, \Delta$ Dalitz decays as well as direct decay of vector mesons ρ, ω and ϕ – are calculated as described in detail in Ref. [52].

The treatment of the 'enhanced' bremsstrahlung contribution from pp, pn as well as πN 'quasi-elastic' scattering, based on the OBE calculations by Kaptari and Kämpfer [41], is discussed in detail in Ref. [40] (cf. Section 2.6 there) where also a discussion of the different models [42–44], which formulate bremsstrahlung in the elementary reactions, can be found. We note here that the OBE models mentioned above [41–44] provide different results not only for the pN bremsstrahlung contribution (which might be attributed to the different way to realize the gauge invariance) but for the Δ -Dalitz decay, due to the different form factors. When comparing the models versus experimental data [37, 38] one has to keep in mind, however, that the descriptions of the bremsstrahlung and of the Δ -Dalitz decay are two decoupled problems in such type of pure phenomenological OBE models. In our transport analysis we use only the bremsstrahlung contribution from [41] and thus, avoid the uncertainties in Δ channel in the OBE models. Also we stress here again that in order to separate the bremsstrahlung ($pp \rightarrow ppe^+e^-$) from a vector-dominance like dilepton production via the ρ -meson ($pp \rightarrow ppp, \rho \rightarrow e^+e^-$), we do not employ a vector-dominance form factor when calculating the bremsstrahlung. Thus, the dilepton radiation via the decay of the virtual photon ($pp \rightarrow pp\gamma^*, \gamma^* \rightarrow e^+e^-$) and the direct ρ decay to e^+e^- are distinguished explicitly in the calculations.

The off-shell HSD transport approach incorporates the *off-shell propagation* for vector mesons as described in Ref. [53] in extension of early BUU transport models [48, 54]. In the off-shell transport description, the hadron spectral functions change dynamically during the propagation through the medium and evolve towards the on-shell spectral functions in the vacuum. As demonstrated in Refs. [20, 40], the off-shell dynamics is important for resonances with a rather long lifetime in the vacuum but strongly decreasing lifetime in the nuclear medium (especially ω and ϕ mesons) and also be proven to be vital for the correct description of the dilepton decay of ρ mesons with masses close to the two pion decay threshold. For a detailed description of the off-shell dynamics and the implementation of in-medium scenarios (as a collisional broadening and/or dropping mass scenario) in HSD as well as for an extension of the LUND string model to include 'modified' spectral functions we refer the reader to Refs. [20, 40, 53]. For the present study we consider the scenario of a 'collisional broadening' of the vector meson spectral functions. This is also supported by experimental data in contrast to the 'dropping mass' scenario (cf. [17–22]).

We use the time integration method to calculate dilepton spectra which means that vector mesons and resonances can emit dileptons from their production ('birth') up to their absorption ('death'). This is especially important for the study of in-medium effects because this method takes the full in-medium dynamics into account .

We note that it is very important to have an adequate description of the elementary reactions, especially near the threshold where the cross sections grow very rapidly. This rise has a big impact on the description of the experimental data. The comparison of the latest experimental data from the HADES collaboration on pp collisions at 3.5 GeV [55]

with HSD calculations shows that the previous parametrizations of η -meson and of vector mesons (ρ, ω) production cross sections from Ref. [40] overestimate the data. The over-prediction of the dilepton yield at the ρ -peak has been already realized in Ref. [40] from the comparison to the DLS data for pp at 2.09 GeV . Thus, we have modified the HSD model accordingly in order to obtain a better description of the existing experimental data on elementary reactions (cf. the discussions in the next subsection).

We note that the HSD model is well tested with respect to the bulk observables at low energy and in light systems, relevant for present study. The pion and eta production from $C + C$ collisions at the energies considered here are shown in Section 3 of Ref. [40].

1. Particle production from elementary reactions

Here we describe the major changes/improvements made in the HSD model used here compared to the basic HSD version 2.5 used for the dilepton analysis in Ref. [40]:

1) The high energy part of the $pp \rightarrow \eta X$ and the $pn \rightarrow \eta X$ cross sections have newly been parametrized. The new parametrization, compared to the experimental data, is shown in Fig. 1 for pp and pn reactions as a function of the centre of mass energy above threshold ($\sqrt{s} - \sqrt{s_0}$). The solid and dashed lines represent the inclusive $pp \rightarrow \eta X$ and $pn \rightarrow \eta X$ cross sections from the HSD model. The experimental data are collected from Refs. [55–59]: the full squares and the open star stand for the exclusive $pp \rightarrow \eta pp$ data, the dots for $pn \rightarrow \eta pn$ data. The full diamond and the full star show inclusive data for $pp \rightarrow \eta X$. It is important to note that in elementary reactions also a deuteron can be produced in the final state via $pn \rightarrow \eta d$. The cross section for this channel is indicated by the dashed-dotted line in Fig. 1, whereas the dotted line shows the $pn \rightarrow \eta X$ cross section including the $pn \rightarrow \eta d$ contribution. The open triangles show the experimental data for $pn \rightarrow \eta d$ from Refs. [56–58]. The channel $pn \rightarrow \eta d$ is not considered in the HSD calculations for $A + A$ and $p + A$ reactions because the probability for deuteron formation in the baryonic medium is negligibly small.

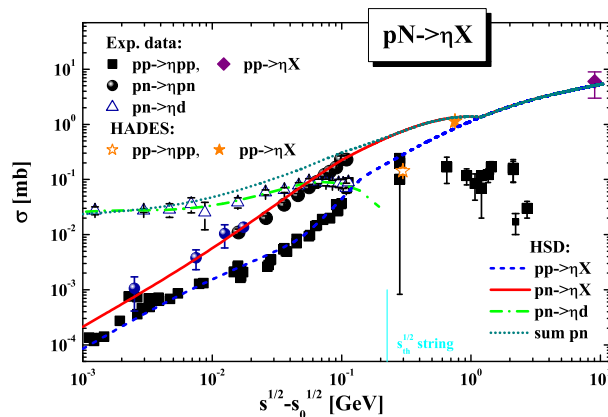


FIG. 1: The η production cross section in pp and pn reactions as a function of the invariant energy above threshold ($\sqrt{s} - \sqrt{s_0}$). The solid and dashed lines represent the inclusive $pp \rightarrow \eta X$ and $pn \rightarrow \eta X$ cross sections from the HSD model, the dashed-dotted line indicates the $pn \rightarrow \eta d$ channel and the dotted line the $pn \rightarrow \eta X$ cross section including $pn \rightarrow \eta d$. The experimental data are collected from Refs. [55–59]: the full squares and open star stand for the exclusive $pp \rightarrow \eta pp$ experimental data, the dots for $pn \rightarrow \eta pn$ and open triangles for $pn \rightarrow \eta d$ experimental data; the solid diamond and solid star show inclusive experimental data for $pp \rightarrow \eta X$.

2) The HSD model has also been improved concerning the isospin separation of the vector meson production in baryon-baryon (BB) and secondary meson-baryon (mB) reactions. The isospin averaged cross sections $BB \rightarrow VB$ ($V = \rho, \omega, \phi$) and $mB \rightarrow VB$ have been replaced by cross sections which take explicitly the isospin for each channel into account. The new parametrization of the cross section as a function of the centre of mass energy, \sqrt{s} for the pp reaction is compared in Fig. 2 to the experimental data. The solid lines represent the parametrizations of the inclusive $pp \rightarrow VX$ ($V = \rho, \omega$) cross sections while the dashed lines stand for the exclusive cross sections. We denote these exclusive cross sections for the ρ -meson production as 'non-resonant' since in this study we consider explicitly the possible contribution of the baryonic resonance $N(1520)$ to the sub-threshold ρ^0 production ($pp \rightarrow N(1520)p \rightarrow \rho^0 pp$).

It is indicated as the dashed-dotted line on the left plot. The dotted line shows the sum of the inclusive 'non-resonant' and exclusive 'resonant' contribution. The experimental data [57, 61, 62] are shown for exclusive $pp \rightarrow Vpp$ (dots) and inclusive $pp \rightarrow VX$ (squares) vector meson production. The stars indicate the inclusive cross section from the HADES collaboration [55].

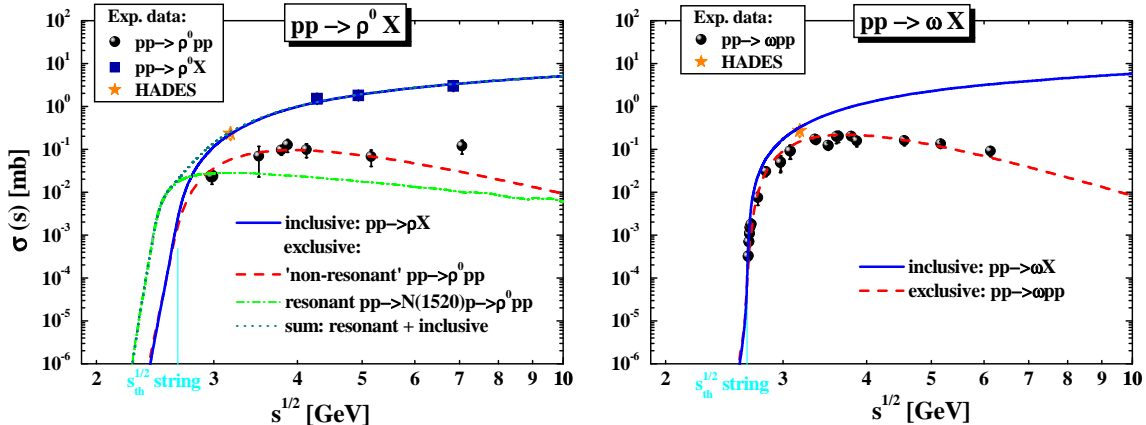


FIG. 2: The production cross sections for the channels $pp \rightarrow \rho X$ (left plot) and $pp \rightarrow \omega X$ (right plot) as a function of the centre of mass energy \sqrt{s} . The solid lines represent the parametrizations of the inclusive $pp \rightarrow VX$ ($V = \rho, \omega$) cross sections while the dashed lines stand for the exclusive 'non-resonant' cross sections. The dashed-dotted line on the left plot shows the contribution from the $N(1520)$ resonance to the ρ^0 production via the process $pp \rightarrow N(1520)p \rightarrow \rho^0 pp$ and the dotted line indicates the sum of the inclusive non-resonant and exclusive resonant contributions. The experimental data [57, 61, 62] are shown for exclusive $pp \rightarrow Vpp$ (dots) and inclusive $pp \rightarrow VX$ (squares) vector meson production. The stars indicate the HADES inclusive cross sections from Ref. [55]. The vertical light blue lines show the threshold for meson production by string formation and decay ($\sqrt{s}_{th} = 2.6 \text{ GeV}$) as implemented in HSD for baryon-baryon channels.

We note that we do not propagate explicitly the $N(1520)$ resonance in the HSD approach, rather we consider it as an excitation in the amplitude which enhances the ρ -meson production in NN and πN reactions at sub-threshold energies. The modelling of the $N(1520)$ production in NN collisions is based on a phase space model with a constant matrix element adopted from Ref. [63]. The contribution of the $N(1520)$ to the ρ cross section is included in line with Ref. [11] which has been used in our previous work [33]. The decay channels of the $N(1520)$ resonance are not well established. Especially the disintegration into a ρ is estimated in between 15 -25%. Including this contribution from the $N(1520)$ resonance decay presents an upper estimate for the ρ -meson production in NN and πN reactions at sub-threshold energies. This model assumption can be checked experimentally via an observation of an enhancement of the dilepton yield near the ρ -peak in the elementary reactions at sub-threshold energies. In the case of heavy-ion collisions at low bombarding energies the contribution of the $N(1520)$ resonance to the dilepton spectra can hardly be seen especially not in reactions of the light nuclei as $C + C$ as measured by the HADES collaboration at 1.0 $AGeV$. The Fermi motion modifies the available energy for meson production and due to the rapid rise of the cross section at threshold the inclusive ρ -meson production mechanism starts to dominate, see Fig. 2, even if the nominal energy is below threshold. On the other hand, the $N(1520)$ resonance can be excited by pion-baryon collisions and contribute to the ρ -meson production via the process $\pi N \rightarrow N(1520) \rightarrow \rho N$. The probability of such processes is larger for heavy nuclei collisions but the pion density is relatively small at sub-threshold energies where the possible contribution of $N(1520)$ plays a role. Consequently, the enhancement of the ρ -meson production by accounting for the $N(1520)$ channel is relatively small in the HSD model. This differs from e.g. the UrQMD model [69, 70] where a much larger cross sections for the $N(1520)$ production is used. We will come back to this discussion in Section IV.

3) We improved also the description of multi-meson production (which is dominantly 2-pion production) in the 'transition' energy range between the one pion production threshold, $\sqrt{s}_{th} = 2m_N + m_\pi = 2.014 \text{ GeV}$ (which occurs dominantly via Delta excitation $NN \rightarrow \Delta N$ and decay or by the direct pion production $NN \rightarrow NN\pi$) and the multi-meson production via string excitation and decay above $\sqrt{s}_{th} = 2.6 \text{ GeV}$. In this energy domain 2π production processes like $NN \rightarrow \Delta\Delta$, $NN \rightarrow \Delta N\pi$ and $NN \rightarrow NN\pi\pi$ become important. Here we improve on the isospin decomposition of these channels using the FRITIOF LUND string model as an 'event generator' with the parameters adjusted to reproduce the multi-meson multiplicities. This allows for a smooth transition in the transition energy regime. The excitation function of the multiplicity of the different pions in HSD is shown in Fig.3, on the left hand side for pp collisions, on the right hand side for pn reactions. These multiplicities are compared with the available

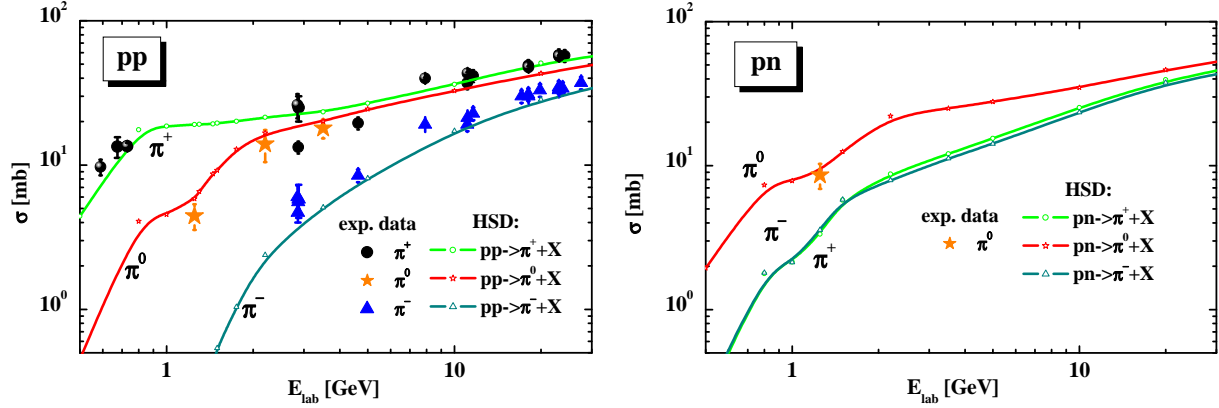


FIG. 3: Left: The inclusive pion production cross sections as a function of the proton bombarding energy E_{lab} . The HSD results are shown in terms of lines with open symbols whereas the experimental data are indicated by the corresponding solid symbols, i.e. for $pp \rightarrow \pi^+ + X$: HSD - the solid line with open dots, experimental data - solid dots from Refs. [61, 76]; for $pp \rightarrow \pi^0 + X$: HSD - the solid line with open stars, the HADES data - full stars from Refs. [55, 60]; for $pp \rightarrow \pi^- + X$: HSD - the solid line with open triangles, experimental data - full triangles from Refs. [61, 76]. Right: The production cross sections for $pn \rightarrow \pi X$, $\pi = \pi^+, \pi^0, \pi^-$ from the HSD model, the HADES data - full star from the extrapolation in Ref. [37].

data which are very scarce for pn reactions.

Additionally to the total pion multiplicity, the multiplicity of Δ 's themselves is very important for the dilepton study because the Δ resonances decay into pions as well as into dileptons whereas other sources of pions do not contribute to the dilepton yield. The Δ production in pp collisions in the HSD approach is shown in Fig. 4 and compared with the available experimental data. Here the production cross sections for the inclusive channels $pp \rightarrow \Delta^+ X$ (solid line) and for the exclusive channel $pp \rightarrow \Delta^+ p$ (dashed line) from HSD are presented as a function of the invariant energy \sqrt{s} . The experimental data [61] are shown for exclusive $pp \rightarrow \Delta^+ p$ production. The star indicates the extrapolation for the Δ inclusive cross section from the dilepton spectra by the HADES collaboration based on the PLUTO simulation program from Ref. [55]. One can see from Fig. 4 that the inclusive Δ production dominates the exclusive one already at relatively low \sqrt{s} . However, due to the lack of inclusive experimental data on Δ production it is hard to justify the modeling of Δ dynamics beyond the exclusive channels which are relatively well known experimentally and accurately modeled in transport approaches.

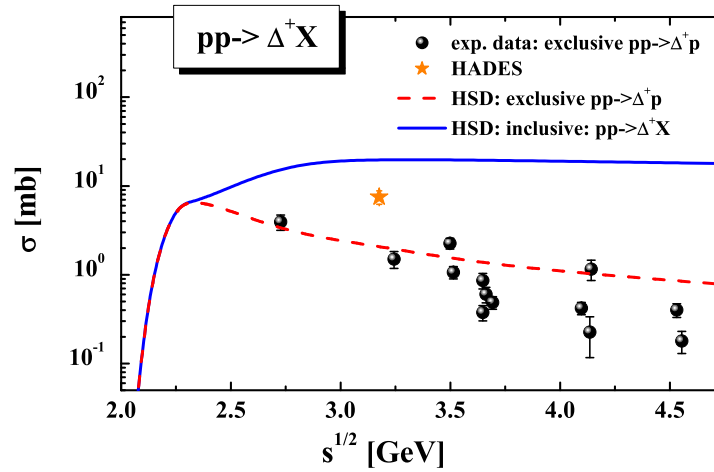


FIG. 4: The production cross sections for the inclusive channels $pp \rightarrow \Delta^+ X$ (solid line) and the exclusive channel $pp \rightarrow \Delta^+ p$ (dashed line) from HSD as a function of the invariant energy \sqrt{s} . The experimental data [61] are shown for exclusive $pp \rightarrow \Delta^+ p$ production. The star indicates the HADES inclusive cross sections from Ref. [55].

B. Open questions related to the elementary reactions in transport models

In nucleon-nucleon collisions at low energies, i.e. below $\sqrt{s} < 2.2 \text{ GeV}$, very seldom more than one meson is produced. The cross sections for these reactions have been measured experimentally (cf. [57]) and are used in the transport approach. Above $\sqrt{s} \approx 2.2 \text{ GeV}$ the multi-meson production starts to dominate, but the experimental information on inclusive as well as exclusive multi-meson production channels are very poor. Also it is not known whether the mesons are directly produced or whether they are decay products of intermediate resonances or strings. The theoretical analysis of these data has not produced yet a consistent knowledge on the channel decomposition [64–67]. This introduces large uncertainties for the prediction of the dilepton yield in transport theories because it depends on the formation of specific intermediate resonances. We note that in the UrQMD model the production of mesons at intermediate energies is realized exclusively via excitation and decay of heavy baryonic resonances which are explicitly propagated in the transport model [69, 70], whereas in HSD the string mechanism is used (as discussed above) for the description of the same final meson spectra. Thus, one needs more exclusive experimental information in order to differentiate between the models.

C. The IQMD model

The IQMD model used for the calculations in this study is the same as introduced in the first IQMD paper on dilepton production [45]. In this model all pions are produced by the decay of Δ resonances. Because no higher mass resonances are included we limit the prediction to beam energies up to 2 AGeV . The excitation function of the pion yield for the $Ca + Ca$ system, compared with the available data, is shown in Fig. 5. We see that the pion multiplicity, the result of a complicated interplay between Δ creation, absorption and decay, is quite reasonable reproduced by the IQMD approach [74]. This is also the case for heavier systems [75]. Thus both, the IQMD as well as the HSD approach, describe the available pion data quite well, a prerequisite for an analysis of the dilepton spectra which are not only normalized to the pion yield but have an important contribution from the Δ decay. For other models which are used to describe the dilepton production, like [68], it remains to be seen whether they reproduce heavy-ion pion data.

For the calculations of the dilepton spectra the standard IQMD program [71, 72] has been supplemented with all elementary cross sections which are important for this process [45]. For that we have used the parametrizations of available experimental data, but for many channels, pp data are only available for low \sqrt{s} values and np data are very scarce. Consequently, in heavy-ion collisions at beam energies larger than 1.5 AGeV most of the particles which emit dileptons are produced using theoretically calculated cross sections. In Ref. [45] we have studied how the uncertainties of the cross sections from elementary reactions influence the dilepton spectra in heavy-ion collisions.

In the IQMD approach the dileptons are calculated perturbatively using the 'spontaneous decay' method - contrary to the time integration method in HSD and UrQMD. It is based on the assumption that all hadrons which decay into dileptons and which are produced in the heavy-ion collision contribute to the dilepton yield as if they were produced in free space. This implies that a possible later reabsorption of the hadrons is not taken into account. Because in reality some of the Δ 's and of the other dilepton producing hadrons are reabsorbed, the IQMD calculations give an upper limit for the dilepton production in heavy-ion collisions. Consequently, the spontaneous decay method limits the approach to small systems contrary to the time integration method which follows the in-medium dynamics of all dilepton sources exactly. However, for the systems studied here the 'spontaneous decay' method is still acceptable. For the details of the cross sections for the creation of dilepton producing particles we refer to Ref. [45].

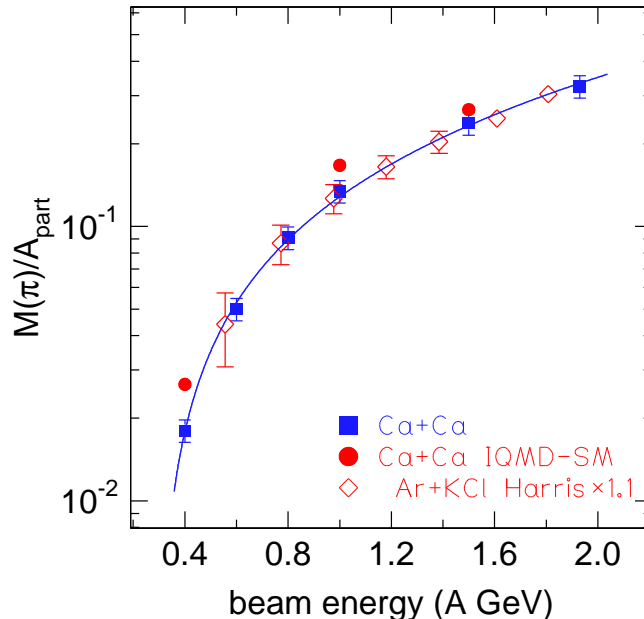


FIG. 5: The excitation function of the π multiplicity per participating nucleon ($(N(\pi^+) + N(\pi^-))/A_{part}$) for Ca+Ca collisions using A_{part} as $0.9A$. Data of the FOPI collaboration are compared with data of Harris et al. [73] and predictions of the IQMD model [74, 75].

III. DILEPTON PRODUCTION IN ELEMENTARY pp, pd AND $p + A$ REACTIONS

The first reaction considered here is the dilepton production in elementary reactions like $p + p$, quasi-free $p + n(d)$ and $p + Nb$ reactions.

A. Dilepton production in pp and pd at energies around 1.25 GeV

We start our discussion with the HADES and DLS data at 1.25 GeV. Fig. 6 shows the differential cross section $d\sigma/dM$ for dileptons as a function of the invariant mass M for pp (left), pn (middle) and pd (right) reactions at 1.25 GeV. The HSD results are presented in comparison to the experimental data from the HADES collaboration [37, 38]. The different lines display the contributions from the various channels in the HSD calculations (for the colour coding we refer to the legend). We note here (and that applies to all further plots) that the theoretical calculations passed through the appropriate experimental acceptance filters and that the mass/momentum resolution is taken into account.

As seen in the left part of Fig. 6 the pp dilepton yield is dominated by the Δ -Dalitz decay while bremsstrahlung is sub-leading due to the destructive interference between initial and final state amplitudes in case of equal charges due to a different sign in the acceleration. Thus these HADES data provide a solid constraint on the Δ production whose control will be very important for a robust interpretation of the heavy-ion data. In pn collisions, however, bremsstrahlung is dominating as can be seen from the middle part of Fig. 6. Because the form of the dilepton invariant mass spectrum from Δ decay and from bremsstrahlung is not completely the same, the form of the pp and the pn spectra is not identical and we see in np a slight enhancement close to the kinematic limit. In the right part of Fig. 6 we compare the HSD results for pd collisions with the so called quasi-free pn HADES data, used later as the 'reference' spectra $NN = (pn + pp)/2$ for the interpretation of the heavy-ion data. Experimentally the quasi-free pn events have been separated by measuring the proton spectator in the pd reactions at $1.6 < p_{lab} < 2.6$ GeV/c.

The comparison of the pp and the $pn(d)$ data shows clearly that in $pn(d)$ the proton does not scatter on a quasi free neutron. The kinematical limit for the invariant mass of the dilepton which is $M_{max} = \sqrt{s_{NN}} - 2m_N = 0.545$ GeV in pp and np collisions is well exceeded in the pd collisions. The largest invariant mass observed ($M \approx 0.66$ GeV) corresponds to the maximal invariant mass which is kinematically allowed in the *three* body pd system under the condition that the outgoing proton has at least a momentum of 1.6 GeV/c. Therefore at the upper end of the invariant mass spectra we have a collision of the proton with the deuteron with a center of mass energy of $\sqrt{s_{pd}} = \sqrt{(p_p + p_d)^2}$.

This observation one has to keep in mind for the interpretation of dilepton production in heavy-ion collisions, when the pd results are used as a reference to discuss the in-medium enhancement of the dilepton yield.

In semiclassical transport calculations, like HSD, one simulates the deuteron as a bound system of a proton and a neutron which are redistributed in coordinate and momentum space according to the wave function of the Paris potential [78]. The energy of each nucleon (in the deuteron rest frame) is taken as $E_N = m_N + \varepsilon/2$, where $\varepsilon = -2.2 \text{ MeV}$ is the binding energy of the deuteron. We use the energy-momentum relation for free particles to determine the effective mass of the nucleon and then the energy-momentum 4-vector to describe the collision. An incoming nucleon scatters with one or subsequently with both nucleons of the deuteron but never with the two at the same time. This gives another kinematics as compared to a true three-body collision and therefore HSD calculations underpredict the dilepton production close to the kinematical limit of pd collisions.

Another problem with the quasi-free pn scattering is related to the possibility of deuteron formation in the final state. This is not probable in heavy-ion collisions (cf. Ref. [79]) and not included in HSD. However, as seen from the Fig. 1, the process $pn \rightarrow \eta d$ might be important for the η -production at threshold energies. Thus, we include this contribution as an enhanced cross section for η production in pn (this was not included in our previous work [40]) but we do not treat the deuteron formation explicitly in the code. As seen from the right part of Fig. 6 in np collisions around $M = 0.4 \text{ GeV}$ the η contribution turns out to be of the same order of importance as Δ -Dalitz decays and bremsstrahlung.

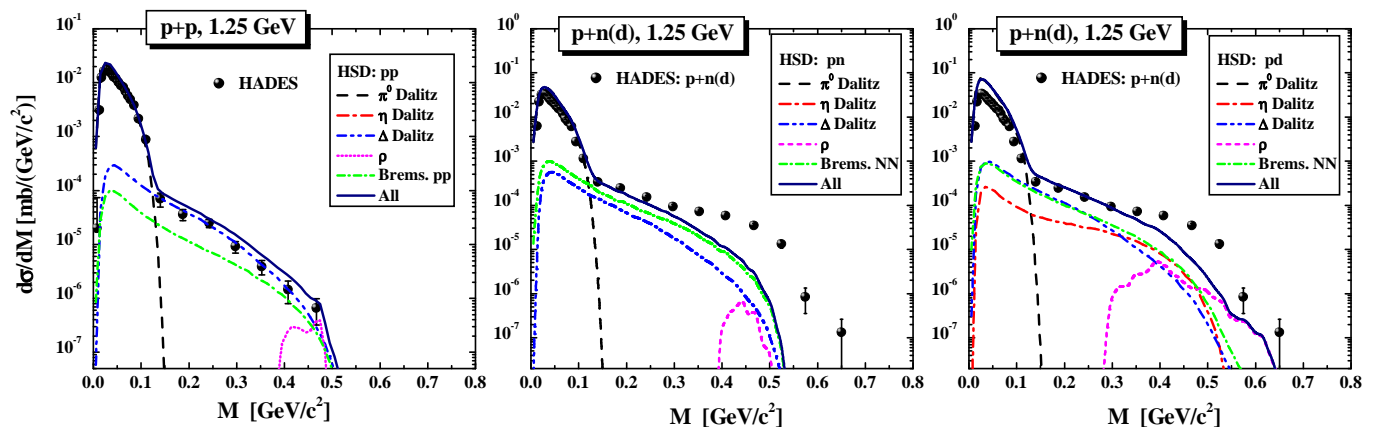


FIG. 6: The HSD results for the dilepton differential cross section $d\sigma/dM$ for pp (left plot), pn (middle plot) and pd (right plot) reactions at 1.25 GeV in comparison to the experimental data for pp (left) and quasi-free pn (middle and right plots) reactions from the HADES collaboration [37, 38]. The individual colored lines display the contributions from the various channels in the HSD calculations (see color coding in the legend). The theoretical calculations passed through the corresponding HADES acceptance filters and mass/momentum resolutions.

Figure 6 (right) shows that in pd collisions the HSD model underestimates the dilepton yield between $0.35 < M < 0.5 \text{ GeV}$, a region which is accessible in two-body collisions at this energy. A possible candidate to explain this enhancement is the contribution of sub-threshold ρ -meson production via excitation and decay of the $N(1520)$ resonance shown as the dashed-dotted line in Fig. 2. A very small contribution of this resonant ρ production channel is even seen in pp collisions (dotted line on the left plot). However, this contribution is not sufficient to describe the experimental data. This is in line with a recent study by the GiBUU group [80]. Also IQMD calculations fail to describe this part of the spectrum.

Fig. 7 shows the IQMD predictions for pp and np collisions as well compared to pp and pd HADES data. We see a very good agreement between HSD and IQMD predictions for the elementary pp and pn reactions.

The cross section $d\sigma/dM$ at 1.27 GeV , calculated in the HSD model, is compared in Fig. 8 to the pp (left) and pd (right) DLS data [24]. The theoretical calculations passed through the corresponding DLS acceptance filter and mass resolution. While the agreement between HSD and the data looks reasonable, one has to keep in mind that due to the very broad mass resolution the spectra are strongly distorted at large invariant masses. There seems to be an underestimation of the last experimental point for pd , however, the quality of the data does not allow for robust conclusions.

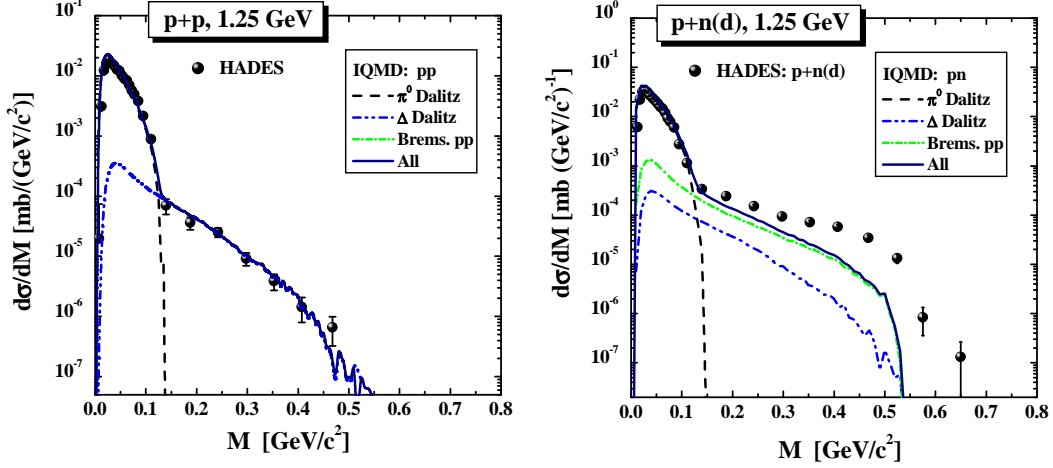


FIG. 7: The IQMD results for the dilepton differential cross section $d\sigma/dM$ for pp (left) and pn (right) reactions at 1.25 GeV in comparison to the experimental data for pp (left) and quasi-free $pn(d)$ (right) reactions from the HADES collaboration [37, 38]. The individual colored lines display the contributions from the various channels in the IQMD calculations (see color coding in the legend). The theoretical calculations passed through the corresponding HADES acceptance filters and mass/momentum resolutions.

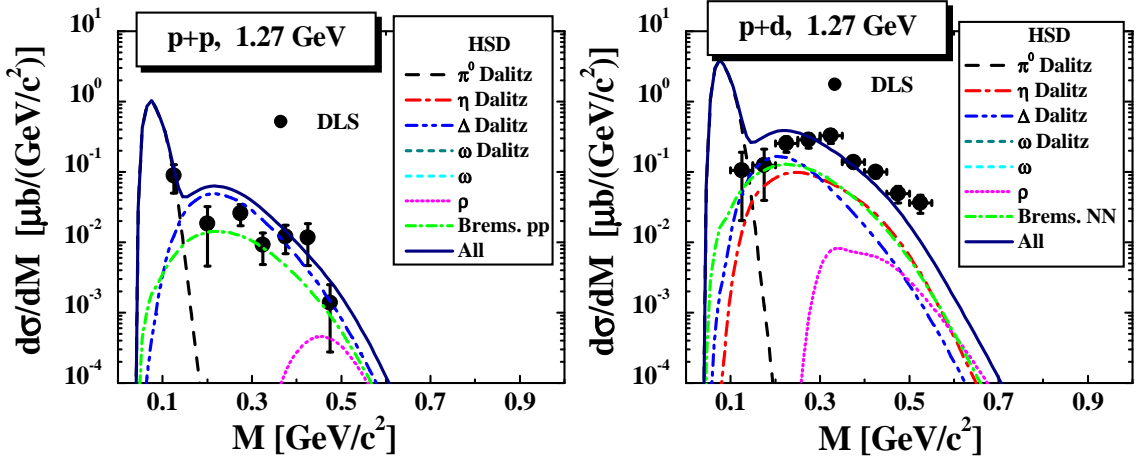


FIG. 8: The dilepton differential cross section $d\sigma/dM$ for pp (left plot) and pd (right plot) at 1.27 GeV in comparison to the DLS data [24]. The HSD calculations passed through the corresponding DLS acceptance filter and mass resolution.

B. Dilepton production in pp and pd at energies around 2.2 GeV

The differential cross section $d\sigma/dM$ from HSD calculations for e^+e^- production in pp reactions at bombarding energies of 2.2 GeV in comparison to the HADES data [60] is presented in Fig. 9 (left). The right part of Fig. 9 shows for the same reaction the HSD results for the differential transverse momentum cross sections for pp at 2.2 GeV separated for different invariant mass bins: $M \leq 0.15$ GeV, $0.15 \leq M \leq 0.55$ GeV and $M \geq 0.55$ GeV. Also at an energy of 2.2 GeV we see a quite satisfying agreement between theory and experiment.

Fig. 10 shows the dilepton differential cross section $d\sigma/dM$ for the pp (left plot) and pd (right plot) at 2.09 GeV from HSD calculations in comparison to the DLS data [24]. We see also here a good agreement and the fact that the DLS as well as the HADES data are reproduced with the same theory underlines the consistency of both data sets which have quite different acceptance cuts.

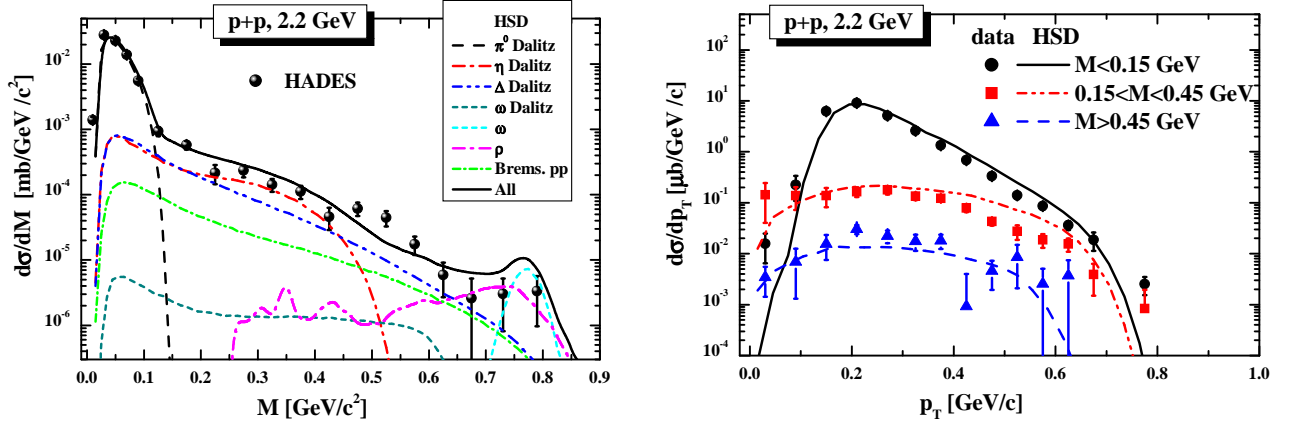


FIG. 9: Left: the differential cross section $d\sigma/dM$ from HSD calculations for e^+e^- production in pp reactions at a bombarding energy of 2.2 GeV in comparison to the HADES data [60]. The individual coloured lines display the contributions from the various channels in the HSD calculations (for the colour coding see legend). Right: HSD results for the differential dilepton transverse momentum cross section for pp at 2.2 GeV and for different mass bins: $M \leq 0.15\text{ GeV}$, $0.15 \leq M \leq 0.55\text{ GeV}$ and $M \geq 0.55\text{ GeV}$. The theoretical calculations passed through the corresponding HADES acceptance filter and mass/momentum resolution.

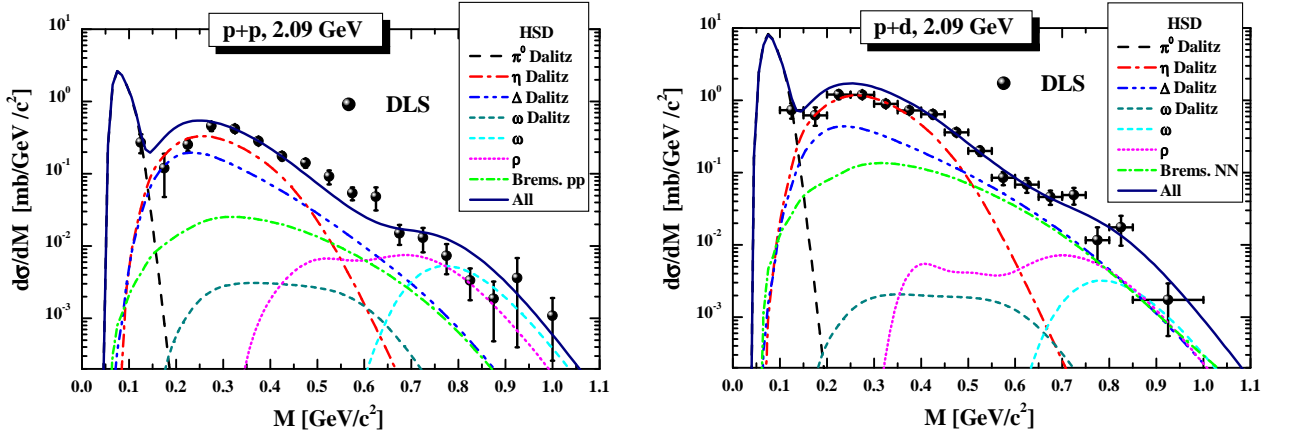


FIG. 10: The dilepton differential cross section $d\sigma/dM$ for the pp (left plot) and pd (right plot) at 2.09 GeV in comparison to the DLS data [24]. The theoretical calculations passed through the corresponding acceptance filters and mass resolutions.

C. Dilepton production in pp at 3.5 GeV

Finally we come to the HADES pp data at 3.5 GeV . Fig. 11 shows the differential cross section $d\sigma/dM$ from HSD calculations for dilepton production in pp reactions at a bombarding energy of 3.5 GeV in comparison to the HADES data [55]. We present the results including and excluding the bremsstrahlung contribution because at this energy there exist no solid bremsstrahlung calculations. The validity of our approach, to take the Kaptari and Kaempfer matrix element and to adjust only the phase space, as described in detail in Ref. [40], becomes questionable at such a high energy. The thick lines, labelled in the legend as "All wo Brems", show the sum of all channels (labelled as "All") without pp bremsstrahlung. For the distribution of the invariant masses of the dileptons, bremsstrahlung does not play a major role at this energy in pp , as expected.

In Fig. 12 we compare the HSD results for pp at 3.5 GeV and for 4 different mass bins: $M \leq 0.15\text{ GeV}$, $0.15 \leq M \leq 0.47\text{ GeV}$, $0.47 \leq M \leq 0.7\text{ GeV}$ and $M \geq 0.7\text{ GeV}$ to the HADES data [55]. The upper 4 plots show the rapidity distribution and the lower 4 plots the transverse momentum spectra. As in Fig. 11 the thick lines, labelled in the legend as "All wo Brems", show the sum of all channels (labelled as "All") without pp bremsstrahlung. We observe that the rapidity distribution is well described except for invariant masses around the ρ peak where we overpredict the data by a constant factor. Also the transverse momentum distribution is well described by theory with the exception of a region around $M \approx 0.6\text{ GeV}$ where our calculations overpredict the data. We speculate that HSD produces slightly too many Δ . Since the elementary cross section for Δ production in pp at this energy is not available, the

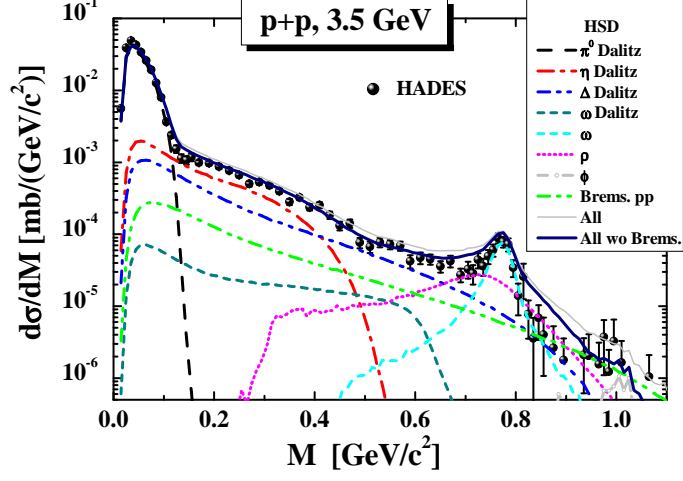


FIG. 11: The differential cross section $d\sigma/dM$ from HSD calculations for e^+e^- production in pp reactions at a bombarding energy of 3.5 GeV in comparison to the HADES data [55]. The individual colored lines display the contributions from the various channels in the HSD calculations (see color coding in the legend). The thick line, labeled as "All wo Brems", shows the total sum of all channels (labeled as "All") without pp Bremsstrahlung. The theoretical calculations passed through the corresponding HADES acceptance filters and mass/momentum resolutions.

repartition of the pion yield between the Δ resonances which produce dileptons and other resonances which do not produce dileptons is not well known and may be the origin of this deviation. For the mass bin $0.47 < M < 0.7\text{ GeV}$ we see that above $p_T = 0.7\text{ GeV}$ bremsstrahlung is the dominating source of dilepton production. We plot the sum of all contributions without bremsstrahlung as well.

D. Dilepton production in pA collisions at 3.5 GeV

We are coming now to $p+A$ reactions. Fig. 13 compares the differential cross section $d\sigma/dM$ from HSD calculations for e^+e^- production in $p+Nb$ reaction at a bombarding energy of 3.5 GeV to the HADES data [77]. The upper part shows the case of the 'free' vector-meson spectral functions while the lower part gives the result for the 'collisional broadening' scenario. Again the thick lines, labeled in the legend as "All wo Brems", show the sum of all channels (labeled as "All") without NN bremsstrahlung. We display both cases since the treatment of bremsstrahlung using the extrapolation of the OBE model to such high energy is questionable, as discussed above. For the same reason the πN bremsstrahlung presented Fig. in 13 has to be considered with care. The collisional broadening scenario comes closer to the experimental results in the region around the ρ peak. We thus find a nice agreement between theory and experiment also for proton-nucleus collisions.

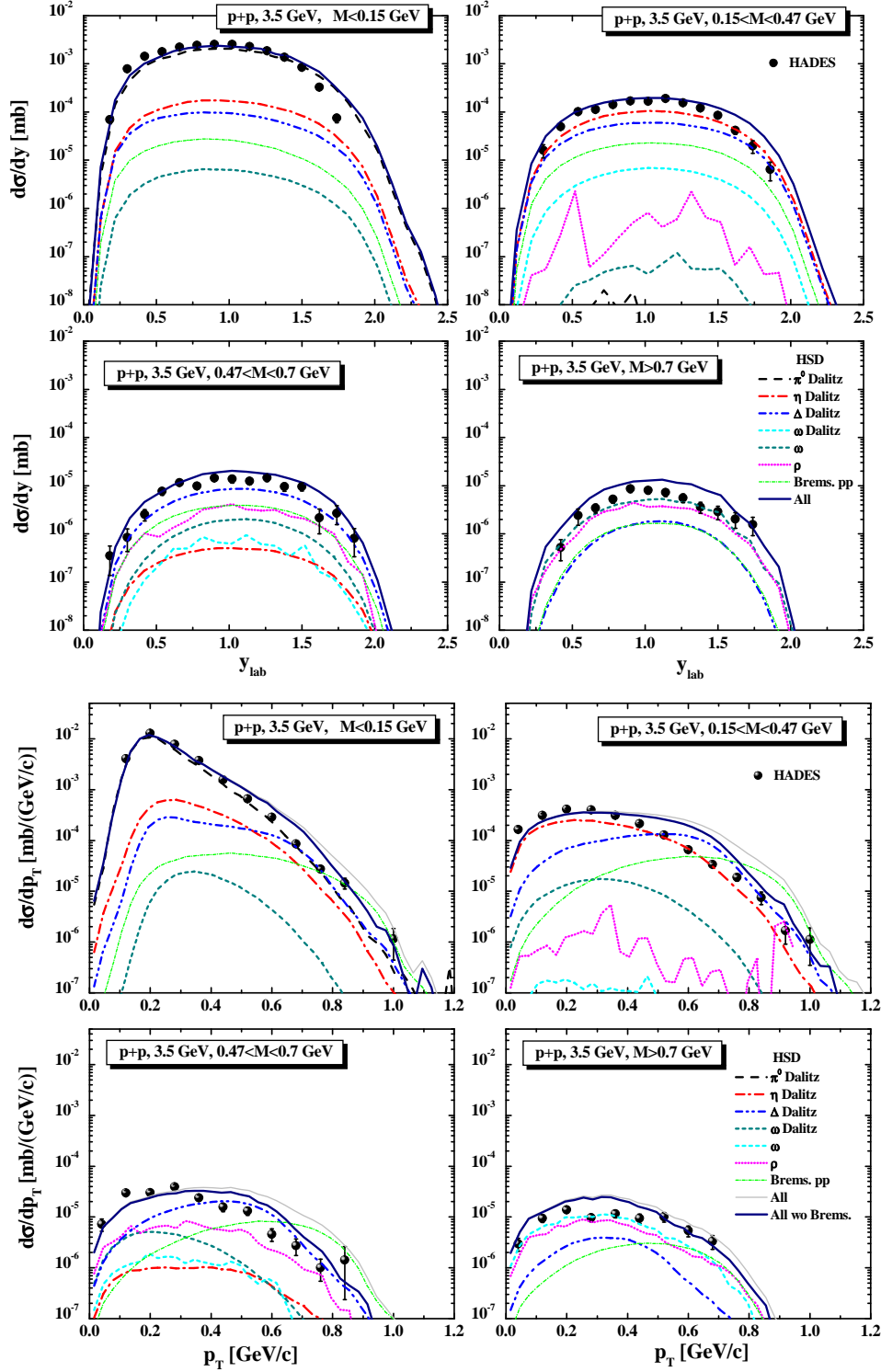


FIG. 12: The HSD results for the rapidity distribution (upper 4 plot) and the transverse momentum spectra (lower 4 plots) for pp at 3.5 GeV and for 4 different mass bins: $M \leq 0.15 \text{ GeV}$, $0.15 \leq M \leq 0.47 \text{ GeV}$, $0.47 \leq M \leq 0.7 \text{ GeV}$ and $M \geq 0.7 \text{ GeV}$ in comparison to the HADES data [55]. The individual coloured lines display the contributions from the various channels in the HSD calculations (see colour coding in the legend). The tick lines, labelled in the legend as "All wo Brems", show the sum of all channels (labelled as "All") without pp Bremsstrahlung. The theoretical calculations passed through the corresponding HADES acceptance filters and mass/momentum resolutions.

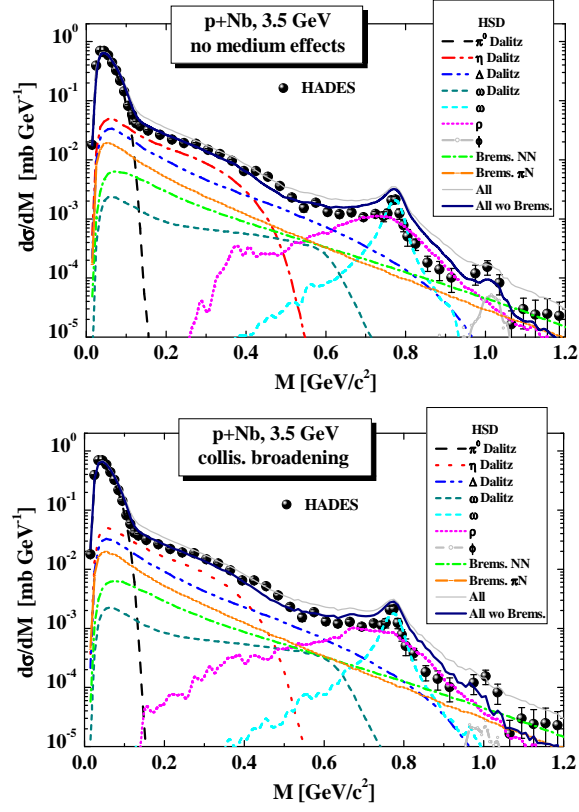


FIG. 13: The differential cross section $d\sigma/dM$ from HSD calculations for e^+e^- production in the $p+Nb$ reaction at a bombarding energy of 3.5 A GeV in comparison to the HADES data [77]. The upper part shows the case of 'free' vector-meson spectral functions while the lower part gives the result for the 'collisional broadening' scenario. The individual coloured lines display the contributions from the various channels in the HSD calculations (see colour coding in the legend). The tick lines, labelled in legend as "All wo Brems", show the sum of all channels (labelled as "All") without pp bremsstrahlung. The theoretical calculations passed through the corresponding HADES acceptance filters and mass/momentum resolutions.

IV. DILEPTON PRODUCTION IN HEAVY-ION COLLISIONS

A. Dileptons from the HSD and IQMD models

Now we come to the heavy-ion results and start with showing in Fig. 14 the mass differential dilepton spectra - normalized to the π^0 multiplicity - of HSD calculations for $C + C$ at 1.0 $AGeV$ in comparison to the HADES data [34]. The HADES collaboration has obtained the π^0 multiplicity by the average of the multiplicity of charged pions [83] and we apply the same method for the theoretical calculations. The upper part displays the results for 'free' vector-meson spectral functions while the lower part shows the result for the 'collisional broadening' scenario. We note here, and this holds for all dilepton spectra normalized to the number of π^0 's, that the normalization is done by the total number of π^0 's in 4π , i.e. without applying an experimental acceptance. This allows for a direct comparison with the published HADES results.

The Δ Dalitz decay and bremsstrahlung contributions are the dominant channels and contribute with about the same weight to the invariant mass spectra. For invariant masses $M > 0.3$ GeV also the subthreshold η channel contributes in an important way. The different descriptions of the ρ meson become important only at large invariant masses where no experimental data are available. The figure shows as well the contribution from direct ρ decays when including the $N^*(1520)$ resonance which may enhance the ρ meson production at sub-threshold energies as discussed in Section II.B. As seen in the figure, there is indeed a small contribution but not larger than the experimental error bars. At higher energies other channels dominate. Therefore the $N^*(1520)$ resonance is not an important source for dilepton production in heavy-ion reactions. Also the 'in-medium' effects due to the collisional broadening of the spectral functions for ρ and ω mesons is not visible in the final spectra due to the strong contributions from other dilepton sources at low invariant masses where this effect is most pronounced and partly due to the limited experimental mass resolution at high invariant masses which smears out the spectra.

Fig. 15 shows the results of IQMD calculations, including acceptance in the same way as the HSD calculations. It is remarkable that the two quite sophisticated transport theories predict results which are that similar. Even the channel decomposition is very similar what is all but trivial because the invariant mass spectra depend on many details of the reaction. They include the Δ dynamics in a nucleus, which we will discuss in section V in more detail, the number of collisions and hence of the spatial distributions of the nucleons in the colliding nuclei, the Fermi momentum and the Pauli blocking of reactions if final state nucleons would be placed in already occupied phase space regions.

Fig. 16 shows the mass differential dilepton spectra - normalized to the π^0 multiplicity - from HSD calculations for $C + C$ - at 2 $AGeV$ in comparison to the HADES data [37]. The theoretical calculations passed through the corresponding HADES acceptance filters and mass/momentum resolutions which leads to a smearing of the spectra at high invariant mass and particularly in the ω peak region. The upper part shows again the case of 'free' vector-meson spectral functions while the lower part presents the result for the 'collisional broadening' scenario. Also here the difference between the in-medium scenarios is of minor importance, partly due to the limited mass resolution which smears out the spectra. Nevertheless, one can conclude that the 'free' calculations predict an enhancement in the region of the ρ mass which is not seen in the experimental data, which are more in favor to the collisional broadening scenario.

Fig. 17 compares the same data with the results from IQMD calculations for $C + C$ - at 2 $AGeV$ which have been acceptance corrected in the same way as the HSD data. Again we see a very good agreement between the two theoretical approaches. Only the different parametrizations of the ω cross section yield deviations at invariant masses around 0.77 GeV .

Fig. 18 displays the mass differential dilepton spectra - normalized to the π^0 multiplicity - from HSD calculations for $Ar + KCl$ at 1.76 $AGeV$ in comparison to the HADES data [39]. The upper part shows again the case of 'free' vector-meson spectral functions while the lower part gives the result for the 'collisional broadening' scenario. Also in this data set the enhancement around the ρ mass is clearly visible.

Fig. 19, which presents the IQMD results for this reaction, shows that the agreement between both theories continues also for heavier systems. Again up to invariant masses of 0.7 GeV both invariant mass spectra are almost identical and agree with data. Also the channel decomposition is rather similar.

The transverse momentum spectra - normalized to the π^0 multiplicity - for $Ar + KCl$ at 1.75 $AGeV$ have been measured by the HADES collaboration for 5 different mass bins [39] : bin 1: $M \leq 0.15$ GeV , bin 2: $0.13 \leq M \leq 0.3$ GeV , bin 3: $0.3 \leq M \leq 0.45$ GeV bin 4: $0.45 \leq M \leq 0.65$ GeV and bin 5: $M \geq 0.65$ GeV . Fig. 20 presents the HADES data in comparison with HSD calculations; on the top without medium effect, on the bottom for the dropping mass scenario. We see also here a good agreement between theory and experiment. Thus one can conclude that the agreement between theory and experiment (Fig. 14 - Fig. 20) up to $M \approx 0.5$ GeV is of such a quality that we can use the theory to study the physical processes involved.

The HADES collaboration has recently measured also the dilepton invariant mass spectra for the reaction Au+Au at 1.25 $AGeV$. The analysis is not completed yet. Fig. 21 presents the HSD predictions for the mass differential

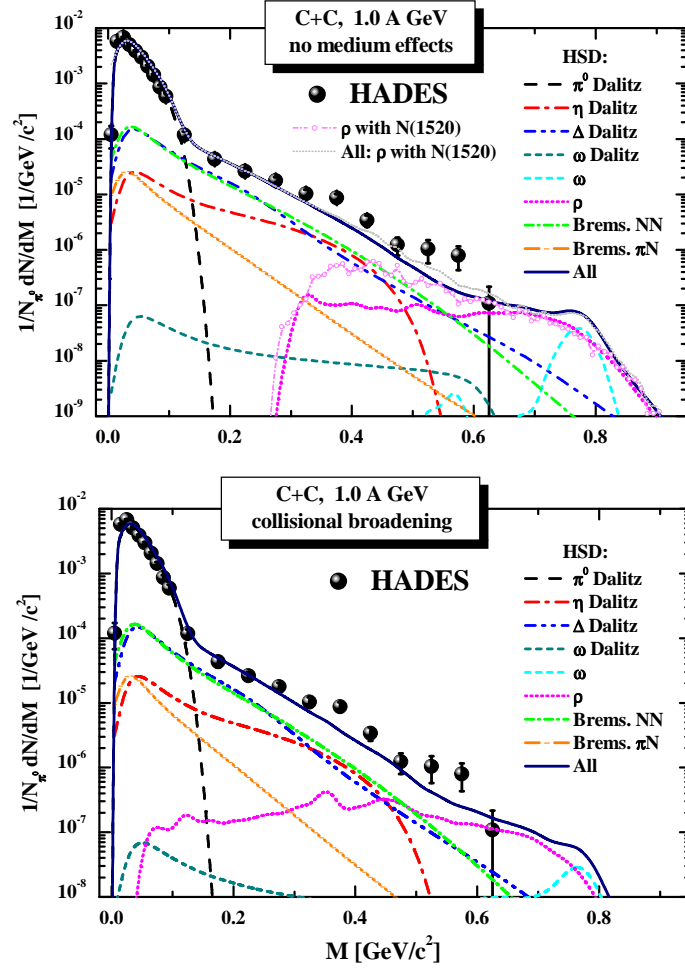


FIG. 14: The results of the HSD transport calculation for the mass differential dilepton spectra - normalized to the π^0 multiplicity - for $C + C$ at 1.0 A GeV in comparison to the HADES data [34]. The upper part shows the case of 'free' vector-meson spectral functions while the lower part gives the result for the 'collisional broadening' scenario. In both scenarios the HADES acceptance filter and mass/momentum resolution have been incorporated. The different color lines display individual channels in the transport calculation (see legend).

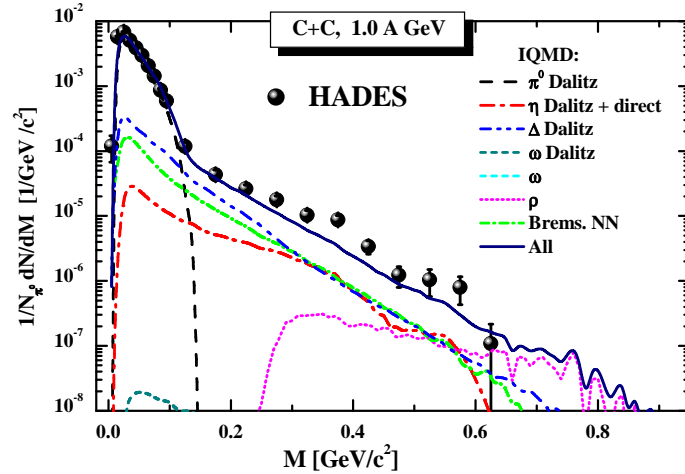


FIG. 15: The mass differential dilepton spectra - normalized to the π^0 multiplicity - from IQMD calculations for $C + C$ - at 1 A GeV in comparison to the HADES data [34]. The different colour lines display individual channels in the transport calculation (see legend). The theoretical calculations passed through the corresponding HADES acceptance filter and mass/momentum resolutions.

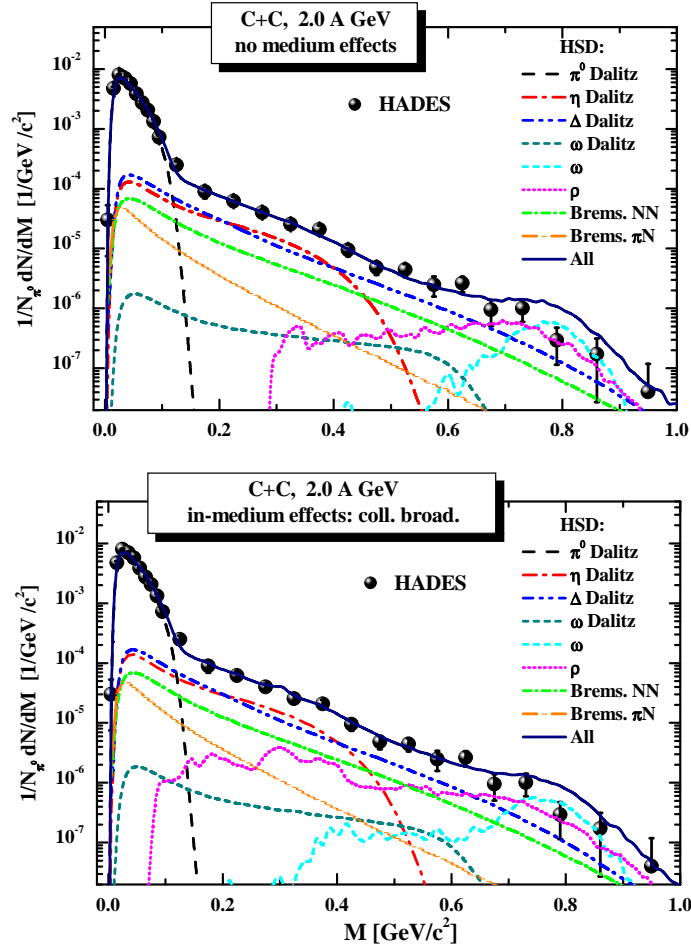


FIG. 16: The mass differential dilepton spectra - normalized to the π^0 multiplicity - from HSD calculations for $C + C$ at 2 $A\text{GeV}$ in comparison to the HADES data [37]. The upper part shows the case of 'free' vector-meson spectral functions while the lower part gives the result for the 'collisional broadening' scenario. The different colour lines display individual channels in the transport calculation (see legend). The theoretical calculations passed through the corresponding HADES acceptance filter and mass/momentum resolutions.

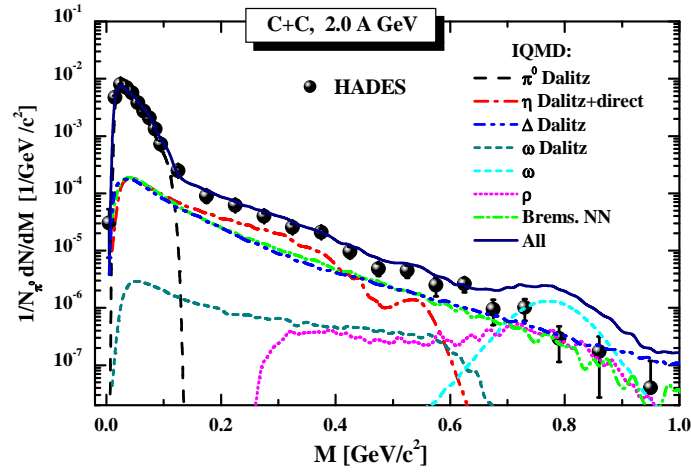


FIG. 17: The mass differential dilepton spectra - normalized to the π^0 multiplicity - from IQMD for $C + C$ at 2 $A\text{GeV}$ in comparison to the HADES data [37]. The different colour lines display individual channels in the transport calculation (see legend). The theoretical calculations passed through the corresponding HADES acceptance filter and mass/momentum resolutions.

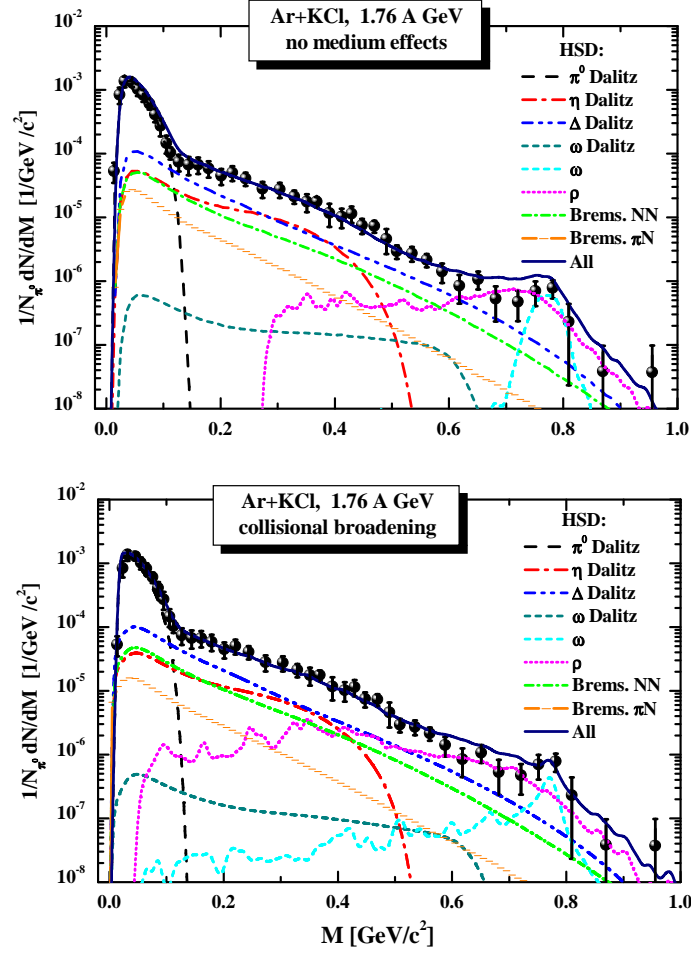


FIG. 18: The mass differential dilepton spectra - normalized to the π^0 multiplicity - from HSD for $Ar + KCl$ at 1.76 A GeV in comparison to the HADES data [39]. The upper part shows the case of 'free' vector-meson spectral functions while the lower part gives the result for the 'collisional broadening' scenario. The individual colored lines display the contributions from the various channels in the HSD calculations (see color coding in the legend). The theoretical calculations passed through the corresponding HADES acceptance filter and mass/momentum resolutions.

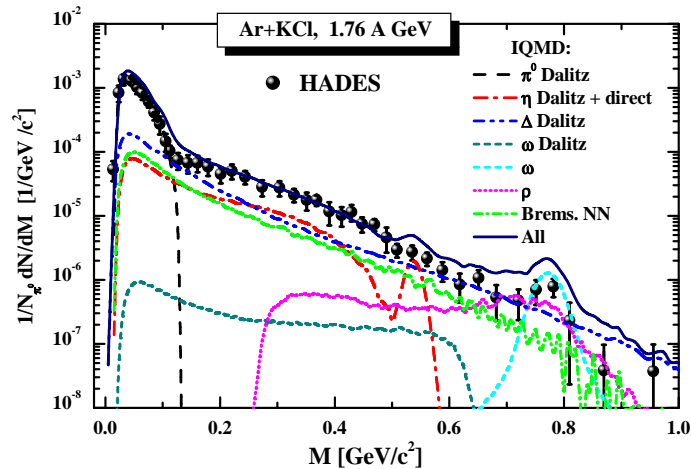


FIG. 19: The mass differential dilepton spectra - normalized to the π^0 multiplicity - from IQMD for $Ar + KCl$ at 1.76 A GeV in comparison to the HADES data [39]. The individual colored lines display the contributions from the various channels in the IQMD calculations (see color coding in the legend). The theoretical calculations passed through the corresponding HADES acceptance filter and mass/momentum resolutions.

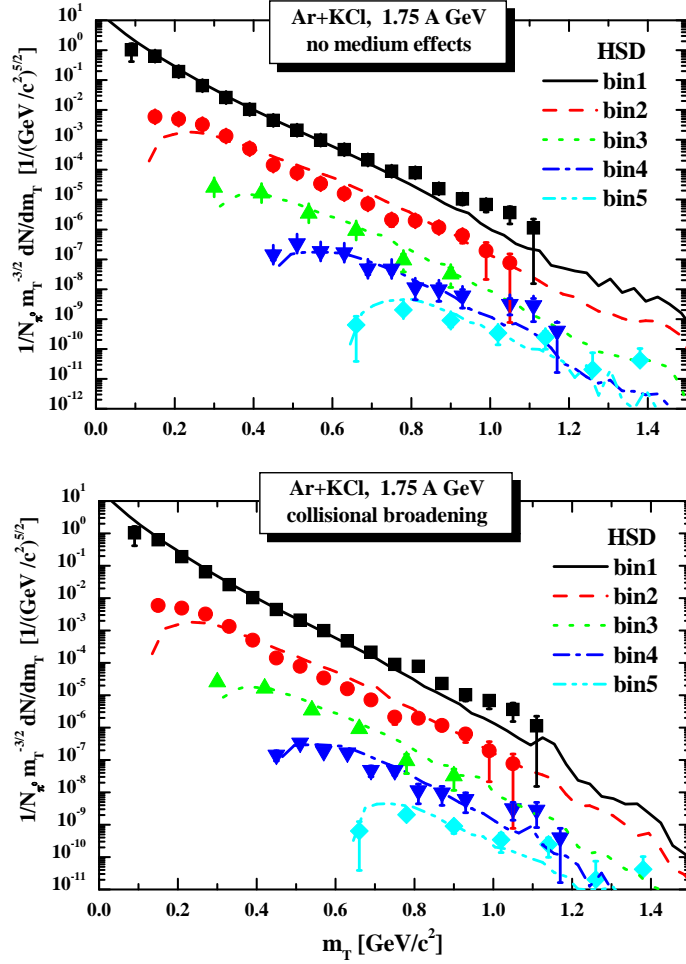


FIG. 20: The HSD results for the transverse momentum spectra - normalized to the π^0 multiplicity - for $Ar + KCl$ at 1.75 $AGeV$ for 5 different mass bins: bin 1: $M \leq 0.15 GeV$, bin 2: $0.13 \leq M \leq 0.3 GeV$, bin 3: $0.3 \leq M \leq 0.45 GeV$ bin 4: $0.45 \leq M \leq 0.65 GeV$ and bin 5: $M \geq 0.65 GeV$ in comparison to the HADES data [39]. The upper part shows the case of 'free' vector-meson spectral functions while the lower part gives the result for the 'collisional broadening' scenario. The individual coloured lines display the contributions from the various channels in the HSD calculations (see colour coding in the legend). The theoretical calculations passed through the corresponding HADES acceptance filter and mass/momentum resolutions.

dilepton spectra - normalized to the π^0 multiplicity - for this reaction. The upper part shows the case of 'free' vector-meson spectral functions while the lower part gives the result for the 'collisional broadening' scenario.

B. Dileptons from the UrQMD model

In this subsection we present the results from the UrQMD (v. 2.3) transport model [69, 70]. As mentioned before, this model, originally designed for ultrarelativistic energies, contains no bremsstrahlung channels and therefore a quantitative comparison with data is not possible. It is nevertheless useful to verify whether it agrees with HSD and IQMD calculations as far as other dilepton sources are concerned. For the details of the dilepton treatment in UrQMD at SIS energies we refer the reader to Ref. [81] where predictions for dilepton spectra from $C + C$ at 2 $AGeV$ have been made, too.

Fig. 22 shows the mass differential dilepton spectra - normalized to the π^0 multiplicity - from UrQMD calculations for $C + C$ - at 2 $AGeV$ in comparison to the HADES data [37] and Fig. 23 - for $Ar + KCl$ at 1.76 $AGeV$ in comparison to the HADES data [39]. As one can see from Figs. 22 and 23 the UrQMD v. 2.3 substantially overestimates the dilepton yield from the vector mesons. The problem can be traced back to the description of ρ production in elementary NN collisions which proceeds via an excitation and decay of heavy baryonic resonances $N(1520), N(1770), \dots$. Their coupling to the ρ channel is not well known and may therefore be overestimated. On the other hand the dilepton yield

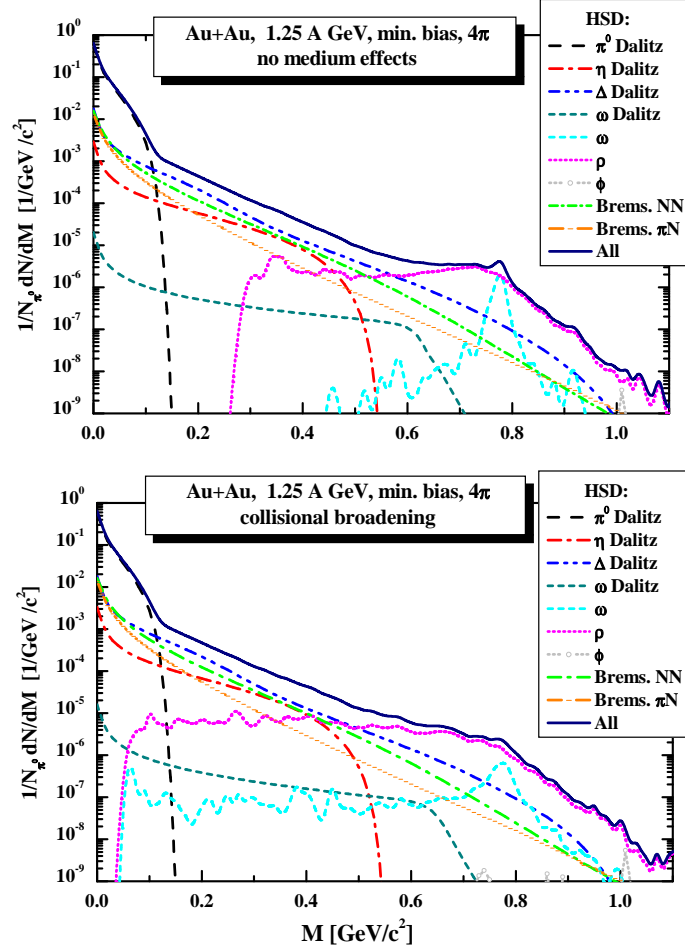


FIG. 21: The mass differential dilepton spectra - normalized to the number of π^0 's - from HSD for minimal bias $Au + Au$ collisions at 1.25 $AGeV$. The upper part shows the case of 'free' vector-meson spectral functions while the lower part gives the result for the 'collisional broadening' scenario. The different color lines display individual channels in the transport calculation (see legend).

at low invariant masses is underestimated for both systems. This is, first of all, due to the lack of the bremsstrahlung contributions but also due to an underprediction of the η yield in UrQMD.

We note that the UrQMD model is presently under improvement and extension updated results for the dileptons at SIS energies are expected soon [82].

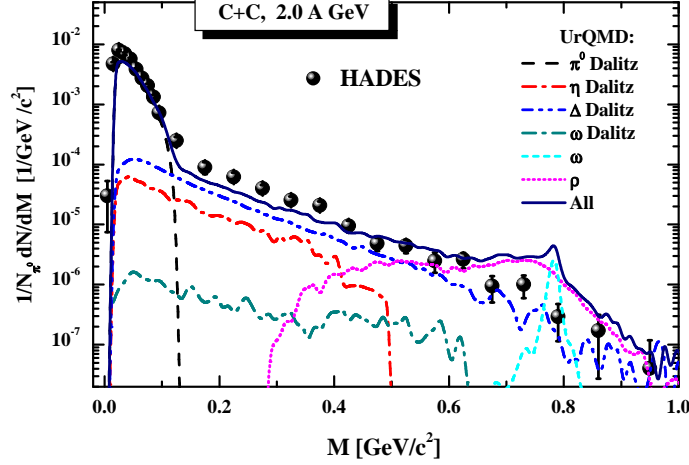


FIG. 22: The mass differential dilepton spectra - normalized to the number of π^0 's - from UrQMD for $C + C$ - at 2 AGeV in comparison to the HADES data [37]. The different colour lines display individual channels in the transport calculation (see legend). The theoretical calculations passed through the corresponding HADES acceptance filter including mass/momentum resolutions.

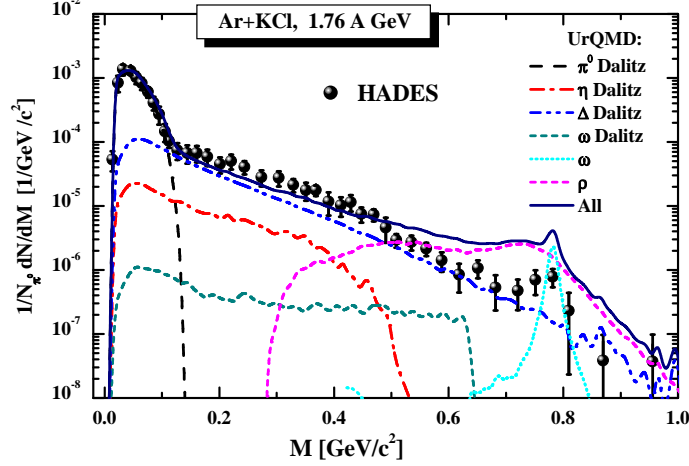


FIG. 23: The mass differential dilepton spectra - normalized to the number of π^0 's - from UrQMD for $Ar + KCl$ at 1.76 AGeV in comparison to the HADES data [39]. The individual colored lines display the contributions from the various channels in the HSD calculations (see color coding in the legend). The theoretical calculations passed through the corresponding HADES acceptance filter including mass/momentum resolutions.

V. RATIOS OF DILEPTON YIELDS $R(AA/NN)$

A. Comparison with experimental data

The primary interest of measuring dilepton production in heavy-ion collisions is to see whether it is a mere superposition of the production in elementary ($pp + pn(d)$) collisions. Of course in this threshold energy regime the Fermi motion of the nucleons inside a nucleus plays an important role and therefore the question has to be formulated more precisely: Is there an in medium enhancement beyond the Fermi motion? This question we will address in this section.

The HADES collaboration has measured the elementary reactions at different beam energies than the heavy-ion reactions. For addressing this question we have, therefore, first to show that the measured ratio for spectra at different energies agrees with the theoretical calculation. Then, in the next subsection, we have to take advantage of the good agreement between data and calculations and compare theoretical calculations of elementary and heavy-ion reactions at the same energy. All calculations presented here have been performed with free vector meson spectral functions.

Fig. 24, left, shows the mass differential dilepton spectra - normalized to the multiplicity of π^0 's and after η Dalitz yield subtraction - from HSD calculations for $C + C$ at 1.0 AGeV (solid line), for the isospin-averaged reference

spectra $NN = (pp + pn)/2$ at 1.25 GeV (short dashed line) and at 1.0 GeV (dashed line) as well as for pd at 1.25 GeV (dot-dashed line). These calculations are compared to the corresponding HADES data from Refs. [37] - for $C + C$ at 1.0 AGeV and the 'reference' spectra taken as an averaged sum of pp and quasi-free $pn(d)$ (denoted as $(pp + pn(d))/2$) measured at 1.25 GeV. The theoretical calculations passed through the HADES acceptance filter for $C + C$ at 1.0 AGeV (denoted as "acc:CC@1AGeV") and mass/momentum resolutions which smears out the high mass region. The theoretical reference spectra is taken as the averaged sum of dilepton spectra from $p + p$ and free $p + n$ collisions. As seen from the figure there is no essential difference between our theoretical pd and NN spectra up to $M \approx 0.5$ GeV and only for larger invariant masses the enhanced 'open' phase space for pd compared to NN becomes important.

Fig. 24 (r.h.s.) shows the ratio of the dilepton differential spectra for $C + C$ at 1.0 AGeV to the isospin-averaged $NN = (pp + pn)/2$. Both spectra are normalized to the π^0 multiplicity and the η Dalitz yield has been subtracted. The solid and short dashed line present the ratio of $C + C$ at 1.0 AGeV to NN at 1.25 GeV in the acceptance region and in 4π , respectively. The dash-dotted and dashed lines are the corresponding ratios of $C + C$ at 1.0 AGeV to NN at 1.0 GeV. If we divide the spectra of $C + C$ at 1.0 AGeV by the NN spectra at 1.25 GeV the ratio is quite flat, as the experiments show as well. The enhancement in the theory at the upper end of the π^0 peak and hence around $M = 0.15$ GeV comes in about equal parts from bremsstrahlung and Δ Dalitz decay. We observe as well that the acceptance cuts do not change the enhancement. Therefore we can discuss it in the next section using 4π yields. In this figure we display as well that the true enhancement, obtained by comparing $C + C$ and NN at the same energy, is much larger. For 0.125 GeV $< M < 0.3$ GeV it is about a factor of two.

We note that the HADES collaboration used pp and quasi-free $pn(d)$ spectra at 1.25 GeV as a reference $NN^d = (pp + pn(d))/2$ spectrum for the ratios of the dilepton yields from AA to NN . In order to avoid the additional uncertainties of dilepton production in pd collision, a system which cannot be modeled reasonably good in semi-classical approaches, we use the reference spectra $NN = (pn + pp)/2$. As Fig. 24 shows, both methods are equivalent up to invariant masses of $M = 0.4$ GeV. Above this value the ratio increases very fast because in the elementary reactions the limitation due to phase space is more severe than in heavy-ion collisions, where the Fermi motion can provide larger invariant masses. These HSD results are confirmed by the IQMD calculations shown in Fig. 25 in a form equivalent to Fig. 24.

Now we step to the energy 2.0 AGeV. In order to compare the experimental data for $C + C$, measured at two different energies 1.0 and 2.0 AGeV, the HADES collaboration transformed the $C + C$ data measured at 2.0 AGeV to the acceptance of $C + C$ at 1.0 AGeV by using - due to lack of statistics - a one-dimensional transformation (see Ref. [37]). We denote this transformation as "1D - acc : CC@1AGeV" in order to distinguish it from the standard three dimensional filtering procedure using the "3D" (defined above as "acc:CC@1AGeV") experimental acceptance matrix (which depends on M, p_T and y), provided by the HADES Collaboration [85] for the filtering of theoretical 4π results.

Fig. 26 presents for $C + C$ at 2.0 AGeV the same quantities as Fig. 24 for $C + C$ at 1.0 AGeV. The solid line on the left is the result of the HSD calculations, the short dashed line and the dashed dotted line are the isospin-averaged reference spectra $NN = (pp + pn)/2$ at 1.25 GeV and pd at 1.25 GeV. The dashed line is the reference NN spectrum at 2.0 GeV; the corresponding HADES data are taken from Refs. [37]. Note, that the simulated HSD mass distribution for $C + C$ at 2.0 AGeV has been transformed to the corresponding acceptance in the same way as done for the experimental data using the "1D - acc : CC@1AGeV" transformation. Fluctuations introduced by this procedure result in part from the limited statistics of the relevant HADES $C + C$ data set and in part from the necessary re-binning of the latter.

The right part of Fig. 26 shows the ratio of the dilepton differential spectra - normalized to the π^0 multiplicity and after η Dalitz yield subtraction - of $C + C$ at 2.0 AGeV to the isospin-averaged reference spectra $NN = (pp + pn)/2$ taken at 1.25 GeV, applying the $C + C$ at 2.0 AGeV "1D - acc : CC@1AGeV" experimental acceptance (solid line) and for 4π (short dashed line). Also the HSD results for the ratio of $C + C$ at 2.0 AGeV to the reference NN spectra, taken at 2.0 GeV, are shown, including the full "3D"- experimental acceptance (dash-dotted line) and in 4π (dashed line). These results show that the experimental data measured up to an invariant mass of $M \approx 0.5$ GeV are compatible with a ratio of one and hence with no in-medium enhancement. The theoretical results are more complicated. Up to an invariant mass of $M \approx 0.3$ GeV theory predicts a enhancement factor of about 1.8 for 4π . The ratio at the same nominal energy shows this enhancement even up to invariant masses of $M \approx 0.6$ GeV before the influence of the Fermi motion sets in.

The IQMD calculations for $C + C$ at 2.0 AGeV are presented in Fig. 27 which shows the same quantities as Fig. 26. We see that the both model agree quite well and the form of the ratio is identical in both approaches.

Fig. 28 (l.h.s.) displays the mass differential dilepton spectra for $Ar + KCl$ at 1.76 AGeV (solid line) - normalized to the π^0 multiplicity and after η Dalitz yield subtraction. We compare HSD calculations for $Ar + KCl$ at 1.76 AGeV, for the isospin-averaged reference spectra $NN = (pp + pn)/2$ at 1.25 GeV (short dashed line) and at 1.76 GeV (dashed line) as well as for pd at 1.25 GeV (dot-dashed line) to the corresponding HADES data, taken from Ref. [39].

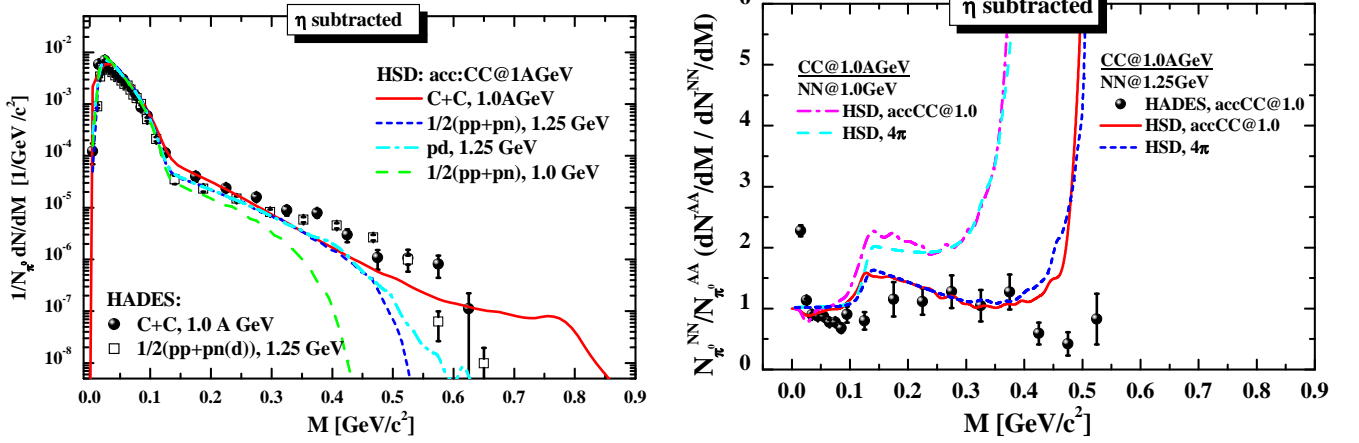


FIG. 24: Left: The mass differential dilepton spectra - normalized to the π^0 multiplicity and after η Dalitz yield subtraction - from HSD calculations for $C + C$ at 1.0 AGeV (solid line), for the isospin-averaged reference spectra $NN = (pp + pn)/2$ at 1.25 GeV (short dashed line) and at 1.0 GeV (dashed line) as well as for pd at 1.25 GeV (dot-dashed line) in comparison to the corresponding HADES data [37] - for $C + C$ at 1.0 AGeV and the 'reference' spectra taken as an averaged sum of pp and quasi-free $pn(d)$ (denoted as $(pp + pn(d))/2$) measured at 1.25 GeV. The theoretical calculations passed through the HADES acceptance filter for $C + C$ at 1.0 AGeV (denoted as "acc:CC@1AGeV") and mass/momentum resolutions. Right: Ratio of the dilepton differential spectra - normalized to the π^0 multiplicity and after η Dalitz yield subtraction - to the isospin-averaged reference spectra $NN = (pp + pn)/2$ taken at 1.25 GeV employing $C + C$ at 1.0 AGeV experimental ("acc:CC@1AGeV") acceptance (solid line) and in 4π (short dashed line). Also the HSD results for the ratio of $C + C$ at 1.0 AGeV to the reference NN spectra at 1.0 GeV are shown with experimental ("acc:CC@1AGeV") acceptance corrections (dash-dotted line) and in 4π (dashed line).

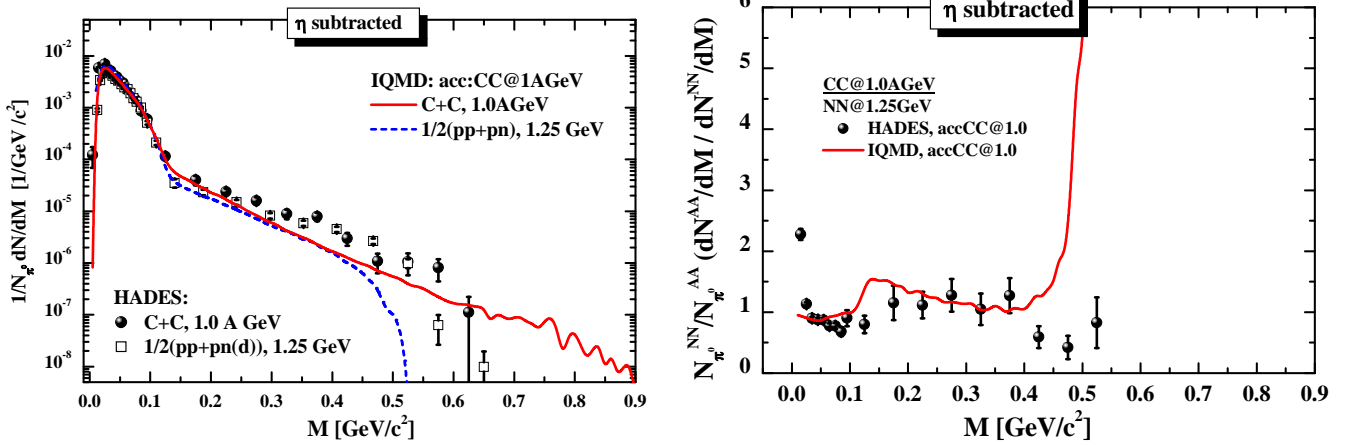


FIG. 25: Left: The mass differential dilepton spectra - normalized to the π^0 multiplicity and after η Dalitz yield subtraction - from IQMD calculations for $C + C$ at 1.0 AGeV (solid line), for the isospin-averaged reference spectra $NN = (pp + pn)/2$ at 1.25 GeV (short dashed line) in comparison to the HADES data [37]. The theoretical calculations passed through the HADES acceptance filter for $C + C$ at 1.0 AGeV and mass/momentum resolutions. Right: Ratio of the dilepton differential spectra - normalized to the π^0 multiplicity and after η Dalitz yield subtraction - of $C + C$ at 1.0 AGeV (employing $C + C$ at 1.0 AGeV experimental ("acc:CC@1AGeV") acceptance) to the isospin-averaged reference spectra $NN = (pp + pn)/2$ taken at 1.25 GeV.

The theoretical calculations for $Ar + KCl$ and for NN passed through the HADES acceptance filter for $Ar + KCl$ and mass/momentum resolutions. The right part of Fig. 28 shows the ratio of the dilepton differential spectra - normalized to the π^0 multiplicity and after η Dalitz yield subtraction - to the isospin-averaged reference spectra $NN = (pp + pn)/2$ taken at 1.25 GeV and employing the $Ar + KCl$ experimental acceptance (solid line) and in 4π (short dashed line). We display as well the HSD results for the ratio of $Ar + KCl$ at 1.76 AGeV to the reference NN

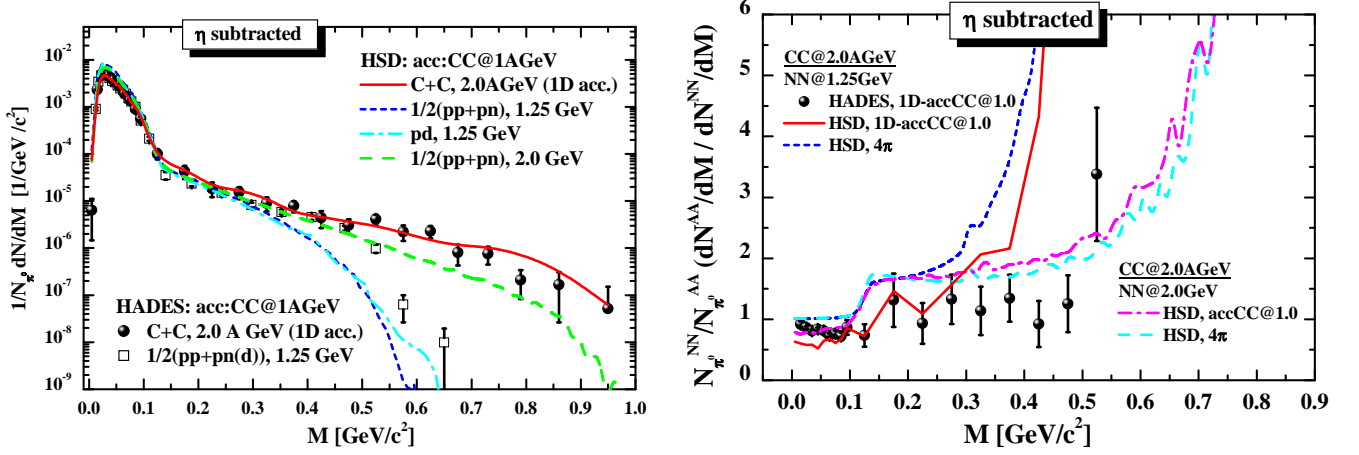


FIG. 26: Left: The mass differential dilepton spectra - normalized to the π^0 multiplicity and after η Dalitz yield subtraction - from HSD calculations for $C + C$ at 2.0 AGeV (solid line) and for the isospin-averaged reference spectra $NN = (pp + pn)/2$ at 1.25 GeV (short dashed line) and at 2.0 GeV (dashed line) in comparison to the HADES data [37] - for $C + C$ measured at 2.0 AGeV and $(pp + pn(d))/2$ at 1.25 GeV and transformed to the acceptance for $C + C$ at 1.0 AGeV (see the discussion in the text). The theoretical calculations passed through the HADES acceptance filter for $C + C$ at 1.0 AGeV ("1D-acc:CC@1AGeV") and mass/momentum resolutions. Right: Ratio of the dilepton differential spectra of $C + C$ at 2.0 AGeV - normalized to the π^0 multiplicity and after η Dalitz yield subtraction - to the isospin-averaged reference spectra $NN = (pp + pn)/2$ at 1.25 GeV with experimental ("1D-acc:CC@1AGeV") acceptance (solid line) and in 4π (short dashed line). Also the HSD results for the ratio of $C + C$ at 2 AGeV to the reference NN spectra at 2.0 GeV are shown: with experimental ("acc:CC@1AGeV") acceptance for $C + C$ at 1.0 AGeV (dash-dotted line) and in 4π (dashed line).

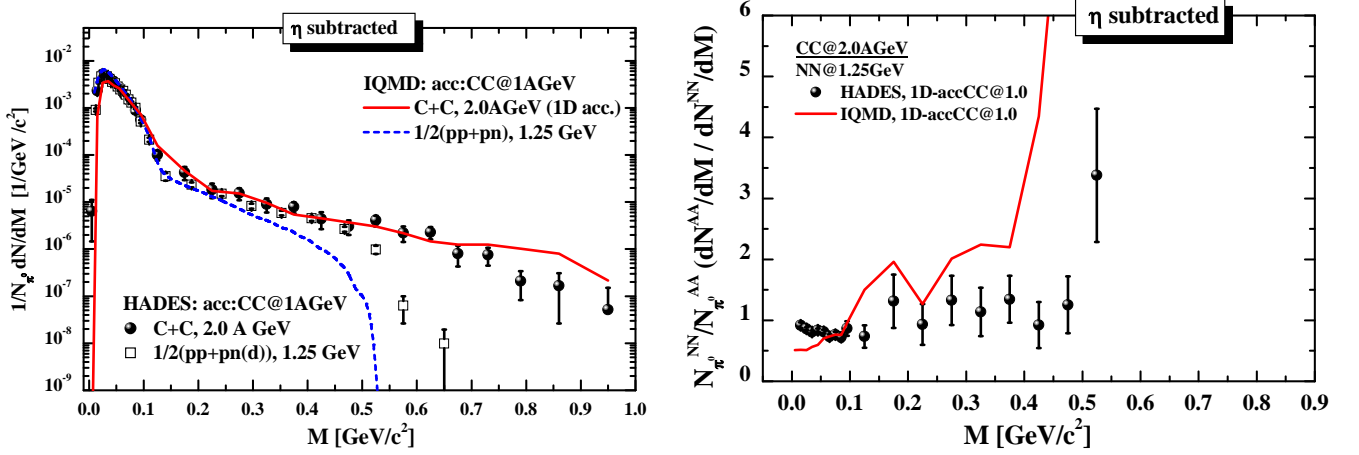


FIG. 27: Left: The mass differential dilepton spectra - normalized to the π^0 multiplicity and after η Dalitz yield subtraction - from IQMD calculations for $C + C$ at 2.0 AGeV (solid line) and for the isospin-averaged reference spectra $NN = (pp + pn)/2$ at 1.25 GeV (short dashed line) in comparison to the HADES data [37]. The theoretical calculations passed through the corresponding HADES acceptance filter for $C + C$ at 1.0 AGeV ("1D-acc:CC@1AGeV") and mass/momentum resolutions (see the discussion in the text). Right: Ratio of the dilepton differential spectra for $C + C$ at 2.0 AGeV - normalized to the π^0 multiplicity and after η Dalitz yield subtraction - to the isospin-averaged reference spectra $NN = (pp + pn)/2$ taken at 1.25 GeV with experimental ("1D-acc:CC@1AGeV") acceptance for $C + C$ at 1.0 AGeV (solid line).

spectrum at the same energy, including the experimental $Ar + KCl$ acceptance (dash-dotted line) and in 4π (dashed line). These results show clearly that for invariant masses of $0.1 \text{ GeV} < M < 0.35 \text{ GeV}$ the data as well as theory are not a mere superposition of the elementary spectra. The comparison also excludes that this enhancement, observed in heavy-ion collisions, is due to acceptance since the results with acceptance and in 4π are very similar. At larger invariant masses theory and data do not agree because of the bump at the invariant masses around $M \approx 0.5 \text{ GeV}$,

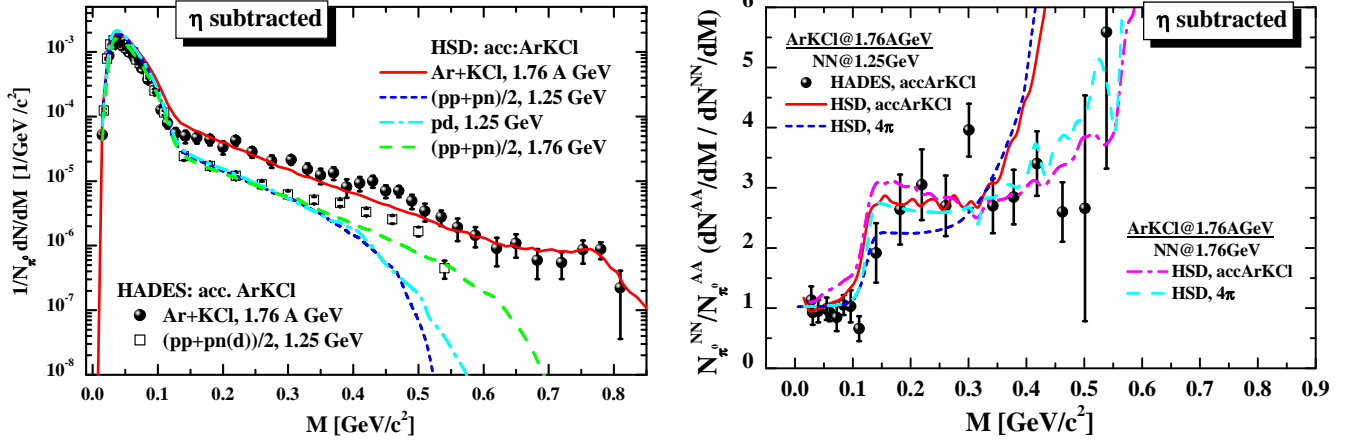


FIG. 28: Left: The mass differential dilepton spectra - normalized to the π^0 multiplicity and after η Dalitz yield subtraction - from HSD calculations for $Ar + KCl$ at 1.76 $AGeV$ (solid line) and for the isospin-averaged reference spectra $NN = (pp + pn)/2$ at 1.25 GeV (short dashed line) and at 1.76 GeV (dashed line) as well as for pd at 1.25 GeV (dot-dashed line) in comparison to the corresponding HADES data [39]. The theoretical calculations for $Ar + KCl$ and for NN passed through the HADES acceptance filter for $Ar + KCl$ and mass/momentum resolutions. Right: Ratio of the dilepton differential spectra - normalized to the π^0 multiplicity and after η Dalitz yield subtraction - to the isospin-averaged reference spectra $NN = (pp + pn)/2$ taken at 1.25 GeV , involving $Ar + KCl$ experimental acceptance (solid line) and for 4π (short dashed line). Also the HSD results for the ratio to the reference NN spectra taken at 1.76 GeV are shown, with the $Ar + KCl$ experimental acceptance (dash-dotted line) and in 4π (dashed line).

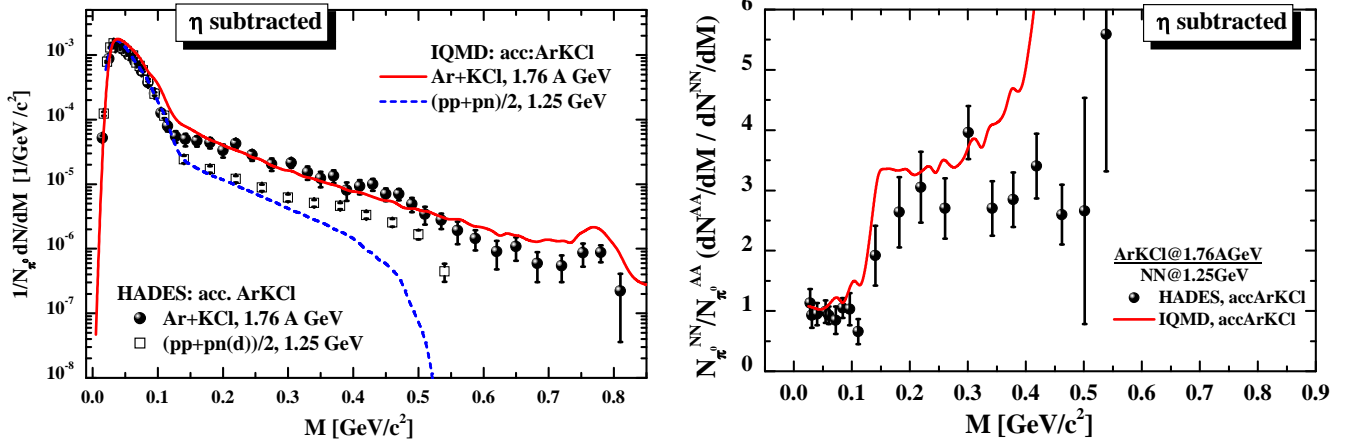


FIG. 29: Left: The mass differential dilepton spectra - normalized to the π^0 multiplicity and after η Dalitz yield subtraction - from IQMD calculations for of $Ar + KCl$ at 1.76 $AGeV$ (solid line) and for the isospin-averaged reference spectra $NN = (pp + pn)/2$ at 1.25 GeV (short dashed line) in comparison to the corresponding HADES data [39]. The theoretical calculations for $Ar + KCl$ and for NN passed through the HADES acceptance filter for $Ar + KCl$ and mass/momentum resolutions. Right: Ratio of the dilepton differential spectra - normalized to the π^0 multiplicity and after η Dalitz yield subtraction - to the isospin-averaged reference spectra $NN = (pp + pn)/2$, taken at 1.25 GeV , employing the $Ar + KCl$ experimental acceptance (solid line).

seen in the experimental pd reactions, is not reproduced by theory. Taking the reference spectra at the same nominal energy theory predicts that this enhancement is constant up to energies of $M \approx 0.5$ GeV . Then the Fermi motion becomes important and yields a strong increase of the ratio.

Consequently, the experimental ratios of the invariant mass spectra measured in heavy-ion collisions to the isospin-averaged reference spectra $NN = (pp + pn)/2$ taken at 1.25 GeV reveals an in-medium enhancement in $Ar + KCl$ collisions at 1.75 $AGeV$ whereas in $C + C$ collisions at 2 $AGeV$ this ratio is compatible with one and therefore no

in-medium enhancement is seen. The transport models show an enhancement in all heavy-ion reactions when the reference spectrum is taken at the same energy. It shows as well that acceptance cuts do not modify this enhancement. The origin of this enhancement will be discussed in the next subsection.

In Fig. 29 we display the same quantities as in Fig. 28 but for IQMD calculations. The enhancement of the experimental ratio is confirmed by IQMD calculations, which are in quantitative agreement with the HSD results.

B. Energy and system size dependence of the dilepton yield

In this section we present the energy and system size dependence of the dilepton yield in 4π as predicted by the HSD calculations in order to study the question of a possible in medium enhancement and to identify eventually its physical origin.

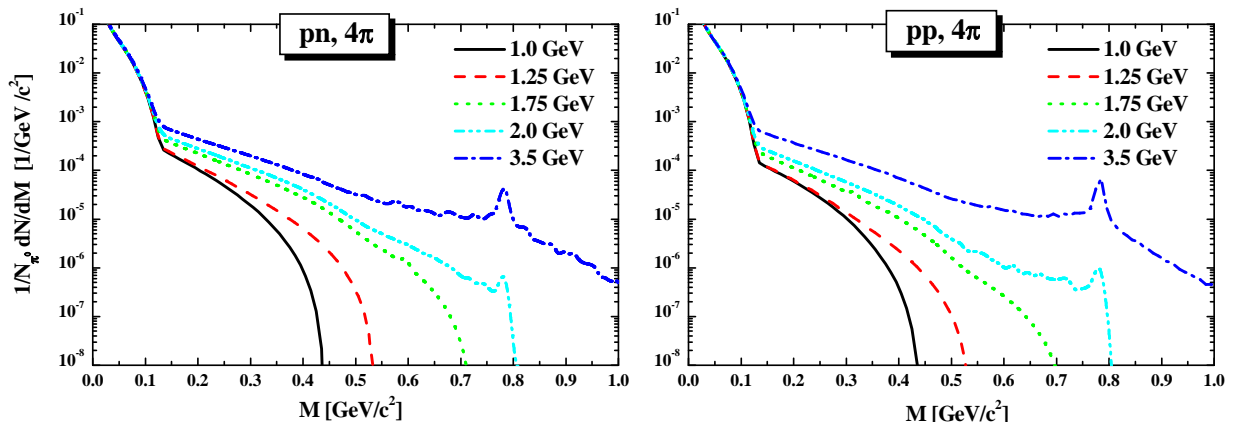


FIG. 30: The 4π mass differential dilepton spectra - normalized to the π^0 multiplicity - obtained in HSD calculations for pn (left) and pp (right) collisions at 1.0, 1.25, 1.75, 2.0 and 3.5 GeV.

Fig. 30 shows the HSD calculations for the mass differential dilepton spectra - normalized to the π^0 multiplicity - for pn (left) and pp (right) collisions at 1.0, 1.25, 1.75, 2.0 and 3.5 GeV in 4π acceptance. Whereas the normalization renders the low invariant mass part to one, independent of the beam energy, the spectra at high invariant masses show a strong beam energy dependence, as expected. Bremsstrahlung is not coupled to the number of pions (or the number of participants which is often assumed to be proportional to the number of π 's) but to the number of collisions. Also the production of heavier mesons increases at these energies close to the meson thresholds, either because it becomes easier to produce them directly or because the baryonic resonances which decay into these resonances are more frequently populated. Last but not least, the phase space limitation of the invariant mass changes with energy which makes ratios between invariant mass spectra at different energies complicated. Due to the isospin dependence of different processes the pp and pn invariant mass spectra differ in detail but are generally determined by phase space. We can conclude from Fig. 30 that the comparison of dilepton data of heavy-ions and of elementary reactions suffer substantially if both are measured at different energies. This renders quantitative conclusions difficult.

Fig. 31 displays the results of HSD calculations for the 4π mass differential dilepton spectra - normalized to the π^0 multiplicity - for the minimal bias symmetric heavy-ion collisions as compared to the isospin-averaged reference spectra $NN = (pn + pp)/2$. We display calculations for $C + C$, $Ar + KCl$, $Au + Au$ at 1.0, 1.25, 1.75, 2.0 AGeV. The upper plot corresponds to the total dilepton $A + A$ spectra whereas the lower plot shows the dilepton spectra after η Dalitz yield subtraction. The thick lines on the lower plot stand for the $A + A$ dilepton yields whereas the thin lines show the NN spectra at the same energies. We see clearly that the dilepton spectra do not scale with the π^0 multiplicity for invariant masses $M > 0.11$ GeV. There is a strong energy and system size dependence of this invariant mass region due to the complicated dynamics of baryon resonances and mesons. Generally the invariant mass spectra in $A + A$ collisions are smoother due to the Fermi motion.

Fig. 32 presents the ratio $(1/N_{\pi^0}^{AA} dN^{AA}/dM)/(1/N_{\pi^0}^{NN} dN^{NN}/dM)$ of the mass differential dilepton spectra - normalized to the π^0 multiplicities - obtained in HSD calculations. Displayed are the ratios of minimal bias $C + C$, $Ar + KCl$, $Au + Au$ collisions and of the isospin-averaged reference spectra $NN = (pn + pp)/2$ at the same energy. The lower plot depicts the same ratios but for the dilepton spectra after η Dalitz yield subtraction. Clearly we see a quite complex structure. We start with the energy dependence of the ratio which decreases with energy. Including the η production this can be clearly seen by comparing the $Au + Au$ collisions at 1.75 and at 1.25 AGeV as well as

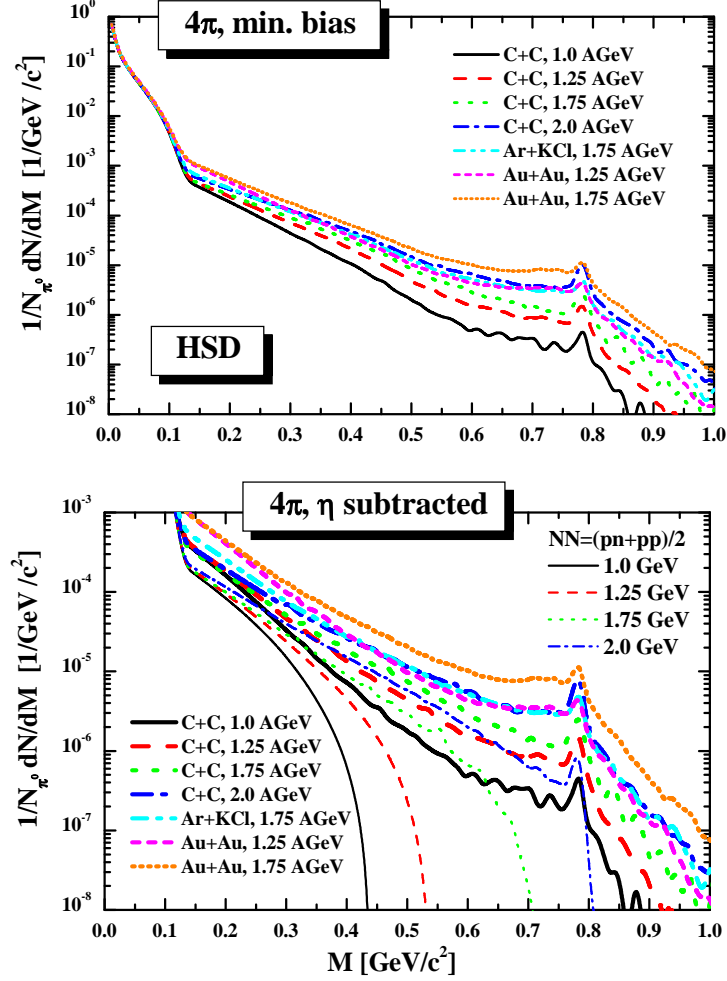


FIG. 31: The invariant mass differential dilepton spectra - normalized to the π^0 multiplicity- obtained in HSD calculations for the minimal bias $C + C$, $Ar + KCl$, $Au + Au$ collisions and for the isospin-averaged reference spectra $NN = (pn + pp)/2$ at 1.0, 1.25, 1.75, 2.0 $AGeV$ in 4π acceptance. The upper plot corresponds to the total dilepton $A + A$ spectra whereas the lower plot shows the dilepton spectra after η Dalitz yield subtraction. The thick lines on the lower plot stand for the $A + A$ dilepton yields whereas the thin lines show the NN spectra at the same energy.

by comparing the $C + C$ system at different energies; η subtraction modifies some details but does not change the tendency. It is also obvious that the ratio increases with the system size. The ratio for $Au + Au$ at 1.25 $AGeV$ is about 4.5, that of $C + C$ at the same energy around 2.5. We study now the origin of this enhancement in detail.

In Fig. 33 we display the enhancement factor in heavy-ion collisions for two different processes: Bremsstrahlung and Δ Dalitz decay. We show the ratio $(1/N_{\pi^0}^{AA} dN^{AA}/dM)/(1/N_{\pi^0}^{NN} dN^{NN}/dM)$ of the dilepton yield from HSD calculations of the minimal bias $A + A$ collisions: $C + C$, $Ar + KCl$, $Au + Au$ and of the isospin-averaged reference spectra $NN = (pn + pp)/2$ at the same energy. The upper part shows the contribution from bremsstrahlung, the lower part that from the Δ Dalitz decay.

We do not expect that bremsstrahlung, one of the dominant sources at beam energies around 1 $AGeV$, scales with the number of pions; therefore the ratio should deviate from one. It has to be systematically larger than one due to multiple collisions of incoming nucleons in heavy-ion collisions. We see that the ratio depends on the mass but little on the energy of the system. In $Au + Au$ collisions where the number of elementary collisions is large the enhancement can reach a factor of 3. At higher energies the bremsstrahlung contribution is not really settled because there are no reliable calculations for the elastic and inelastic elementary channels.

The other dominant source for dilepton production at beam energies around 1 $AGeV$ is Δ Dalitz decay. One may assume that the Δ Dalitz decay scales with the number of pions because the relative ratio is given by the branching ratio but this is not the case. First of all, we are here in a threshold region where the Fermi momentum only can

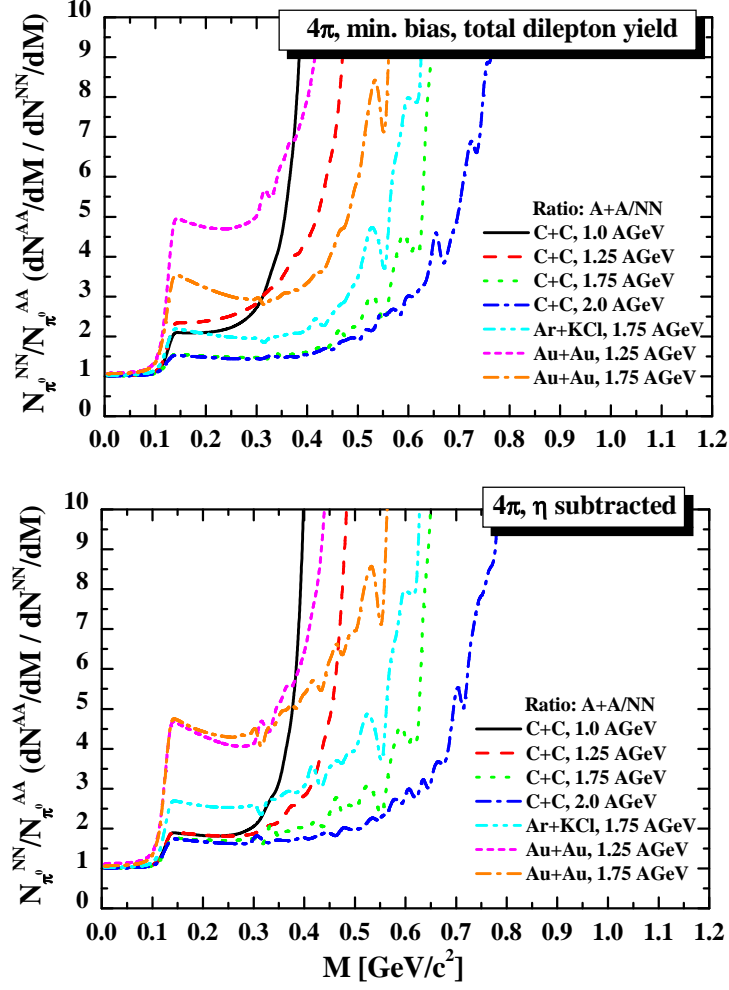


FIG. 32: Upper plot: The ratio $(1/N_{\pi^0}^{AA} dN^{AA}/dM)/(1/N_{\pi^0}^{NN} dN^{NN}/dM)$ of the invariant mass differential dilepton 4π spectra - normalized to the π^0 multiplicity - from HSD calculations for minimal bias $A+A$ collisions: We display $C+C$, $Ar+KCl$, $Au+Au$ collisions in comparison to the isospin-averaged reference spectra $NN = (pn + pp)/2$ at 1.0, 1.25, 1.75, 2.0 $AGeV$. Lower plot: the same ratios but for the dilepton spectra after η Dalitz yield subtraction.

TABLE I: Ratio of π^0 mesons and the integrated dilepton yield ($N(\Delta \rightarrow e^+e^-) = \int dM \frac{dN(\Delta \rightarrow e^+e^-)}{dM}$) from Δ Dalitz decays for $C + C$ and $Au + Au$ at $b=0.5 fm$ and 1 $AGeV$ and that from the 'elementary' NN reactions for different scenarios: with/without Fermi motion ('Fermi m. '), with/without secondary meson-baryon collisions ('mB col.')

1	2	3	4	5	6	7	8
Fermi m.	mB col.	system	$N(\pi^0)$	$N(\Delta \rightarrow e^+e^-)$	$R(\pi^0) = \frac{N^{AA}(\pi^0)}{N^{NN}(\pi^0)}$	$R(e^+e^-) = \frac{N^{AA}(\Delta \rightarrow e^+e^-)}{N^{NN}(\Delta \rightarrow e^+e^-)}$	$\frac{R(e^+e^-)}{R(\pi^0)} = \frac{(7)}{(6)}$
-	-	CC	0.743	$0.565 \cdot 10^{-4}$	6.74	5.56	0.83
-	-	AuAu	18.76	$1.688 \cdot 10^{-3}$	170.08	166.3	0.98
+	-	CC	1.407	$1.16 \cdot 10^{-4}$	12.76	11.42	0.89
+	-	AuAu	31.07	$2.75 \cdot 10^{-3}$	281.69	270.93	0.97
-	+	CC	0.633	$0.86 \cdot 10^{-4}$	5.74	8.47	1.47
-	+	AuAu	10.75	$3.45 \cdot 10^{-3}$	97.46	339.8	3.49
+	+	CC	1.07	$1.77 \cdot 10^{-4}$	9.70	17.44	1.80
+	+	AuAu	16.62	$6.32 \cdot 10^{-3}$	150.68	622.66	4.13

lead to a substantial enhancement of the production. Secondly, pions from Δ decay can be reabsorbed by nucleons and can form again a Δ which may later disappear in a $\Delta N \rightarrow NN$ collisions. This process is even important in systems as small as $C + C$. Dileptons, on the contrary, cannot be reabsorbed and are seen in the detector. Table I shows quantitatively the consequences of these processes for reactions at 1 $AGeV$. We compare there the pion and dilepton yield for $C + C$ and $Au + Au$ for different conditions. If there is neither a Fermi momentum (Fermi m.) nor meson absorption on baryons (mB col.) the ratio of π^0 's to dileptons corresponds to the branching ratios and the enhancement factor (last column) is one, independent of the system size of the heavy-ion reaction. The Fermi motion alone increases the pion yield (6th column) as well as the dilepton yield (7th column) by almost a factor of two. Because in the ratio displayed in Fig. 33 one divides by the number of pions this ratio remains one for small invariant masses whereas the Fermi motion makes the ratio explode for invariant masses close to the phase space boundary. Meson-baryon interactions (mB coll) lower the number of pions in heavy-ion collisions, by 15% in $C + C$ collisions and by 47% in $Au + Au$ collisions because they can lead to a disappearance of the pions if the $\pi N \rightarrow \Delta$ collision is followed by a $\Delta N \rightarrow NN$ collision. At the same time they enhance the dilepton yield because dileptons do not get reabsorbed and therefore every Δ which is produced contributes to the dilepton yield. The meson-baryon interactions are therefore the reason that dileptons behave differently than pions. This cycle of Δ production, Δ decay and π reabsorption in $\pi N \rightarrow \Delta$ collisions, which leads in heavy system to the creation of several generations of Δ 's, has been studied already 20 years ago as one of the key elements to the pion dynamics in heavy-ion collision which allows the pions to equilibrate with the system and to serve as a measure of the number of participants [84]. The last two lines of Table I show that the pion absorption enhances the dilepton production as compared to the pions by a factor of about 1.5-1.7 in $C + C$ collisions and by a factor of 3.5-4.1 for $Au + Au$ collisions, i.e. the enhancement grows with the size of the system.

The system size effect is demonstrated explicitly in Fig. 34: the left plot shows the ratio of the mass differential dilepton spectra $(1/N_{\pi^0}^{AA} dN^{AA}/dM)/(1/N_{\pi^0}^{NN} dN^{NN}/dM)$ - normalized to the π^0 multiplicity and after η Dalitz yield subtraction - from HSD calculations for the minimal bias $C + C, Ar + KCl, Cr + Cr, Ti + Pb, Au + Au$ collisions and of the isospin-averaged reference spectra $NN = (pn + pp)/2$ at 1.75 $AGeV$. The right plot shows the same but for the Δ Dalitz decay contributions only. We see also here that the different ratios are separated by a factor which is (almost) independent of invariant mass and depends basically on the size of the colliding nuclei since the effect of multiple Δ regeneration increases with the atomic number of the colliding ions.

Thus, the dilepton enhancement observed in Fig. 32 (and hence also in the experimental spectra) is due to bremsstrahlung and due to the Δ dynamics in the medium. Both are not related to collective effects like the in-medium modifications of spectral functions but are a mere consequence of the presence of other nucleons in the nuclei. They also appear if no potential but only collisional interactions between the nucleons exist. This effect grows with the nuclear size which is directly related to an increase of the high baryon density phase from light to heavy-ion collisions. This is demonstrated in Fig. 35 which shows the time evolution of the baryon density from HSD in the central cell $\rho(0, 0, 0, t)$ in units of the normal nuclear density $\rho_0 = 0.168 \text{ fm}^{-3}$ for central ($b = 0 \text{ fm}$) $Au + Au$ (left plot) and $Ar + KCl$ (right plot) at different energies - 1.25, 1.7, 2.0 and 3.5 $AGeV$. By comparing the $Ar + KCl$ and $Au + Au$ density profiles one sees that the maximum density reached in the central cell is approximately the same in both cases - up to $3\rho_0$ and only slightly grows with increasing energy. However, the high baryon density phase for the heavy $Au + Au$ nuclei collisions is much longer than for the intermediate $Ar + KCl$ system which implies a longer reaction time and a stronger influence of secondary reactions on observables as discussed above.

C. In-medium effects in vector meson production

Now we come to the question - how the in-medium effects in vector meson production can influence the ratios. The dilepton spectra for $p + Nb$ at 3.5 $AGeV$, $C + C$ at 1.0, 2.0 $AGeV$ and for $Ar + KCl$ at 1.75 $AGeV$ within the collisional broadening scenario for the vector meson spectral functions have been already presented in Sections III and IV (cf. Figs. 13,14,16,18) in comparison to the HADES data as well as our predictions for $Au + Au$ at 1.25 $AGeV$ (cf. Fig. 21).

In Fig. 36 we display for reactions at 1.70 $AGeV$ the system size dependence of the 4π mass differential dilepton spectra - normalized to the π^0 multiplicity - from HSD calculations for minimal bias $A + A$ reactions. We display the result for the symmetric $Cr + Cr$ and $Au + Au$ systems as well as for the asymmetric $Ti + Pb$ system. The solid lines stand for the 'no medium effects' scenario whereas the dashed lines show the dilepton yield for the 'collisional broadening' scenario. The lower plot is a 'zoom' of the upper one for the mass range $0.4 < M < 1.0 \text{ GeV}$. First of all we note the growth of the dilepton yield for $0.15 \leq M \leq 0.6 \text{ GeV}$ when going from the intermediate $Cr + Cr$ to the heavy system $Au + Au$. The larger the system mass, the more important is the aforementioned Δ reaction cycle and the more the dilepton production is enhanced as compared to pion production. As we have discussed already in Sections III and IV, for the collisional broadening scenario one sees clearly the influence of the larger width of the

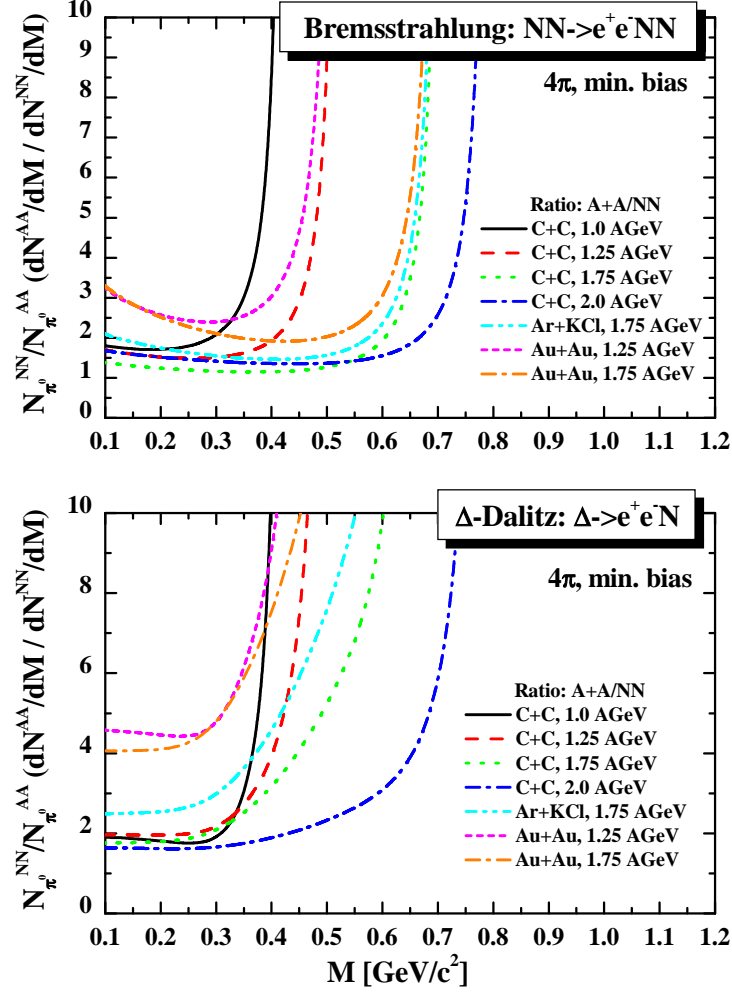


FIG. 33: Upper plot: The ratio $(1/N_{\pi^0}^{AA} dN^{AA}/dM)/(1/N_{\pi^0}^{NN} dN^{NN}/dM)$ of the dilepton yield from the bremsstrahlung channel (upper part) and Δ Dalitz decay (lower part) - normalized to the multiplicity of π^0 . We display HSD calculations for the ratio of the minimal bias $C + C$, $Ar + KCl$, $Au + Au$ collisions and the isospin-averaged reference spectra $NN = (pn + pp)/2$ at the same energy.

vector meson resonances (the peaks get smaller and broader).

What would be the consequence of this in-medium effect on the dilepton ratio of AA spectra to the 'reference spectrum'? Would this observable yield information on the underlying dynamical processes? Previously we concentrated on the ratio $R(AA/NN)$ where the 'reference spectrum' is constructed as an average of pp and pn yields: $NN = (pp + pn)/2$. However, such a ratio would not be well suited for studying in-medium effects in the vector meson mass region due to the limited open phase space in NN collisions relative to AA collisions - taken at the same energies - since the Fermi motion in AA extends the kinematical limits, which leads to a fast rise of $R(AA/NN)$ at larger invariant masses M . Moreover, as has been discussed in Section III.A, there is a general problem with NN as a 'reference spectrum' since experimentally pn are usually quasi-free pd reactions. For the beam energies discussed here, in the interesting invariant mass region, $M > 0.5 GeV$ there are no 'quasi-free' pn collisions anymore but genuine three-body pd collisions.

Alternatively, the in-medium enhancement can be studied by comparing the yield of a heavy system to that of a light system. Fig 37 displays for a beam energy of 1.7 AGeV the ratio of the invariant mass differential dilepton spectra for intermediate $Cr + Cr$ and heavy $Au + Au$ nuclei and of the light nuclei $C + C$, which is chosen as a 'reference spectrum'. We study two scenarios - the 'no medium effects' and the 'collisional broadening' scenario. One clearly sees that the enhancement for $M \leq 0.5 GeV$ due to the multiple Δ production and bremsstrahlung persists when one compares collisions of heavy and light nuclei and can become as large as a factor of two. Thus, $C + C$

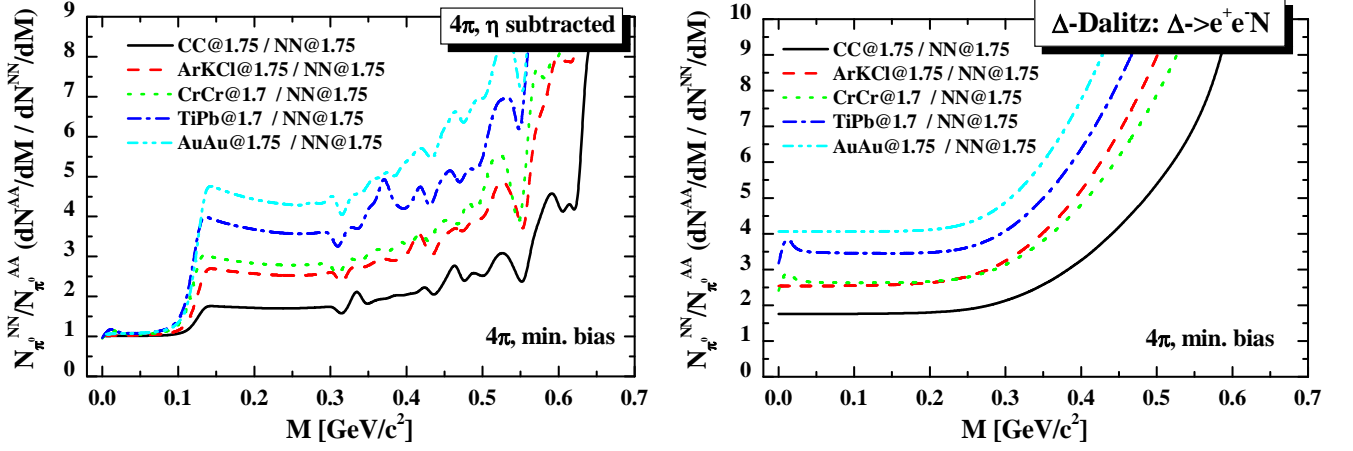


FIG. 34: Left: The 4π ratio $(1/N_{\pi^0}^{AA} dN^{AA}/dM)/(1/N_{\pi^0}^{NN} dN^{NN}/dM)$ of the mass differential dilepton spectra - normalized to the π^0 multiplicity and after η Dalitz yield subtraction - from HSD calculations for the minimal bias $C+C$, $Ar+KCl$, $Cr+Cr$, $Ti+Pb$ and $Au+Au$ collisions to the isospin-averaged reference spectra $NN = (pn + pp)/2$ at 1.75 AGeV. Right: same as the left plot but for the Δ Dalitz decay contributions, only.

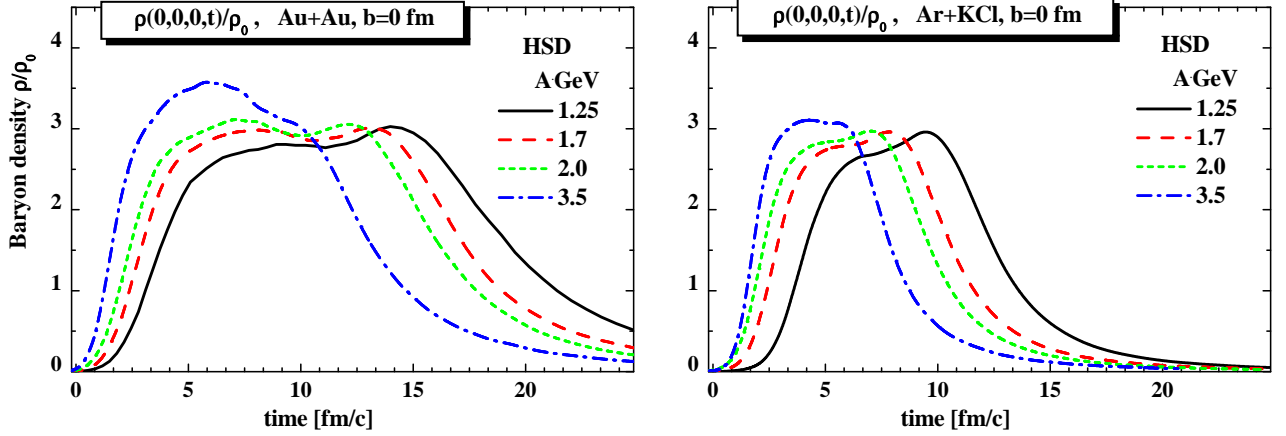


FIG. 35: The time evolution of the baryon density from HSD in the central cell $\rho(0,0,0,t)$ in units of the normal nuclear density $\rho_0 = 0.168 \text{ fm}^{-3}$ for central ($b = 0 \text{ fm}$) $Au+Au$ (left plot) and $Ar+KCl$ (right plot) at different energies - 1.25, 1.7, 2.0 and 3.5 AGeV.

collisions can also be used as 'reference spectra' to study such nuclear effects. Moreover, we observe as well that the difference between the two scenarios is small for low invariant masses and becomes only noticeable at invariant masses close to the ρ mass. However, even there the differences remain moderate. Therefore high precision data are required to study the question whether vector mesons are modified by the strongly interacting medium in this energy region. On the other hand the ratio for $AuAu/CC$ grows much faster (for both - the no medium and the in-medium scenario) than for $CrCr/CC$. This is due to the enhancement of the vector meson productions by secondary meson-baryon and meson-meson interactions in heavy system relative to the light system. This effect is hence easy to observe experimentally.

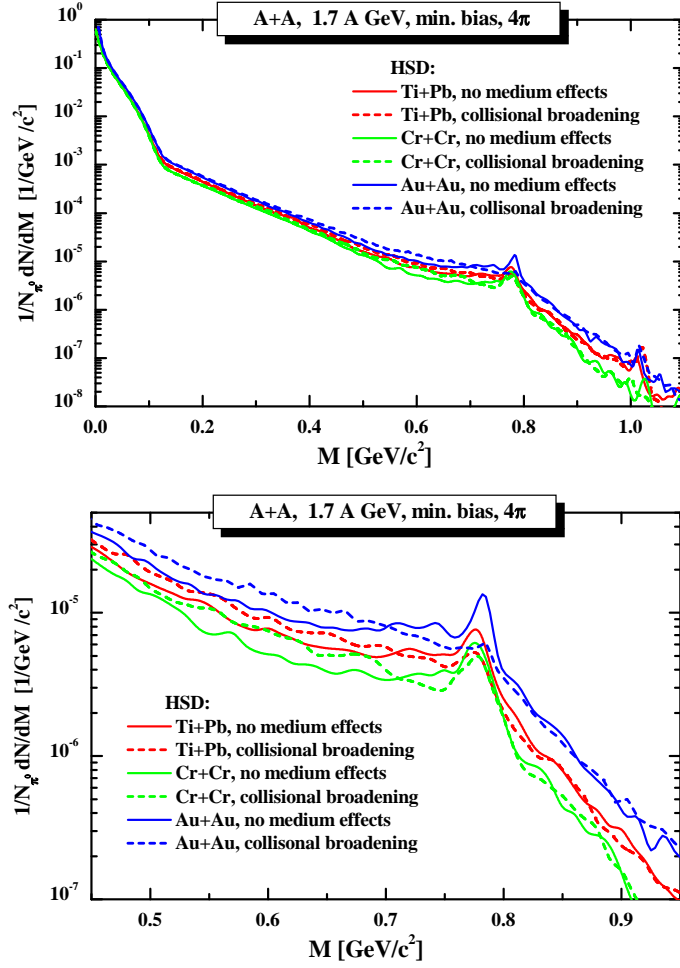


FIG. 36: The 4π mass differential dilepton spectra - normalized to the π^0 multiplicity - from HSD calculations for minimal bias $Ti + Pb$, $Cr + Cr$ and $Au + Au$ collisions at 1.7 A GeV. The solid lines stand for the 'no medium effects' scenario whereas the dashed lines show the dilepton yield for the 'collisional broadening' scenario. The lower plot is a 'zoom' of the upper plot for the mass range $0.4 < M < 1.0$ GeV.

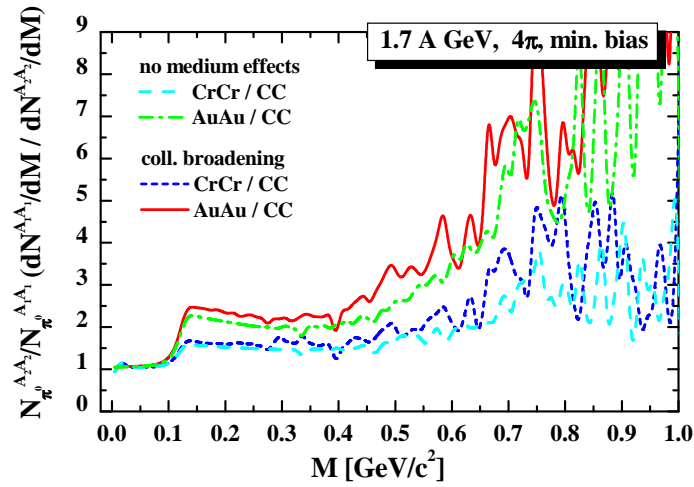


FIG. 37: The 4π ratio $(1/N_{\pi^0}^{A_2 A_2} dN^{A_2 A_2}/dM)/(1/N_{\pi^0}^{A_1 A_1} dN^{A_1 A_1}/dM)$ of the mass differential dilepton spectra - normalized to the π^0 multiplicity - from HSD calculations for minimal bias $Au + Au$ ($Cr + Cr$) collisions and $C + C$ collisions. This ratio is displayed for the 'no medium effects' and for the 'collisional broadening' scenario.

VI. CONCLUSIONS

We have studied the production of dileptons in pp , pn , pA and AA collisions at energies between 1 and 3.5 $AGeV$ by comparing the results of three independent transport approaches - HSD, IQMD and UrQMD - with all existing data in this energy domain. The results of the transport approaches agree well with the data. This allows for the conclusion that the dilepton production in heavy-ion collisions is theoretically sufficiently well understood.

We have shown that the dilepton spectra from elementary reactions can be well described as the superposition of the emission from known dilepton sources. In pp collisions at energies of around 1 GeV dileptons stem dominantly from the Δ Dalitz decay whereas in pn collisions the bremsstrahlung radiation becomes equally important. At higher energies η production sets in and contributes to the invariant mass range $M < 0.55 GeV$. At higher invariant masses the vector meson decays dominate but the data are presently not precise enough to allow for firm conclusions.

Our study demonstrates that the dilepton production from heavy-ion reactions cannot be interpreted as a simple convolution of the average dilepton yield from pn and pp collisions times the number of such elementary collisions. The presence of a nuclear medium manifests itself in several ways: First of all the Fermi motion of nucleons in nuclei smears out the energy distribution of primary NN collisions substantially. This has a big influence on the particle production at (sub-)threshold energies. The Fermi motion enhances the pion as well as the dilepton yields in AA collisions at threshold energies by up to a factor of two. The enhancement is, however, identical for pions and dileptons. Therefore, if one normalizes the dilepton yield to the pion multiplicity, as done in the experimental analysis, no enhancement is observed.

Experimentally an enhancement is seen even if one normalizes the dilepton yield by the π^0 multiplicity. The experimental enhancement is, however, plagued by the use of pd collisions instead of pn collisions because in the interesting kinematical regime the pd collisions are true three-body collisions and cannot be interpreted as quasi-free pn reactions. So the true enhancement – as compared to elementary collisions – cannot be inferred from present data for invariant masses above 0.5 GeV

We have analysed this enhancement in detail and found two origins: The first reason is bremsstrahlung radiation from pn and pp reactions which does not scale with the pion number (i.e. number of participants) rather with the number of elementary elastic collisions. The second reason is the shining of dileptons from the 'intermediate' Δ 's, which take part in the $\Delta \rightarrow \pi N$ and $\pi N \rightarrow \Delta$ reaction cycle. This cycle produces a number of generations of Δ 's during the reaction which increases with the size of the system. At the end only one pion is produced but each intermediate Δ has contributed to the dilepton yield because emitted dileptons do not get absorbed. This leads to an enhancement of the dilepton yield as compared to the final number of pions. Thus, the enhancement confirms the predictions of transport theories that in heavy-ion collisions several generations of Δ 's are formed which decay and are recreated by $\pi N \rightarrow \Delta$ reactions.

We do not find evidence that the observed enhancement of the dilepton yield in heavy-ion collisions over the elementary reactions for $M < 0.5 GeV$ requires the assumption of 'conventional' in-medium effects like a modification of the spectral functions of the involved hadrons. Theory predicts such a modification for vector mesons and the consequences can be seen for invariant masses $M > 0.5 GeV$, however, more precise data are needed to draw robust conclusions on a quantitative level.

We summarize with the final remark that the ratio of dilepton yields AA/NN is a sensitive observable which allows to penetrate the intermediate phase of the heavy-ion reaction and sheds light on the Δ dynamics which is not accessible by the hadronic observables. Moreover, by measuring this ratio at a low bombarding energy one can get access to the bremsstrahlung radiation since it becomes a dominant process there. One expects to observe in this case the scaling of the ratio with the number of binary collisions rather than with the number of pions. A precise measurement of the ratio of dilepton yields in heavy-nuclei collisions (as $Au + Au$ or $Pb + Pb$) and of that in the light systems (as $C + C$) for invariant masses $M > 0.5 GeV$ will help to obtain information on the in-medium modification of the spectral function of vector mesons.

Acknowledgements

The authors are grateful for fruitful discussions with W. Cassing, C. Hartnack, L. Fabietti, M. Gumberidze, F. Krizek, Y. Leifels, O. Linnyk, A. Rustamov, J. Stroth, P. Salabura, H. van Hees and M. Weber. Our special thanks go to T. Galatyuk and R. Holzmann for the continues help and many useful advises concerning the experimental data and filtering procedure. E.B. acknowledges financial support through the "HIC for FAIR" framework of the "LOEWE" program.

-
- [1] Z. Fodor and C. Hoelbling, *Rev. Mod. Phys.* **84** (2012)449.
- [2] G. E. Brown and M. Rho, *Phys. Rev. Lett.* **66** (1991) 2720.
- [3] G. E. Brown, C. H. Lee, M. Rho and V. Thorsson, *Nucl. Phys. A* **567** (1994) 937.
- [4] T. Hatsuda, S. H. Lee and H. Shiomi, *Phys. Rev. C* **52** (1995) 3364.
- [5] M. Asakawa, C. M. Ko, P. Lévai, X. J. Qiu, *Phys. Rev. C* **46** (1992) R1159.
- [6] M. Herrmann, B. Friman, W. Nörenberg, *Nucl. Phys. A* **560** (1993) 411.
- [7] G. Chanfray, P. Schuck, *Nucl. Phys. A* **545** (1992) 271c.
- [8] F. Klingl, W. Weise, *Nucl. Phys. A* **606** (1996) 329; F. Klingl, N. Kaiser, W. Weise, *Nucl. Phys. A* **624** (1997) 527
- [9] R. Rapp, G. Chanfray and J. Wambach, *Phys. Rev. Lett.* **76** (1996) 368.
- [10] R. Rapp, G. Chanfray and J. Wambach, *Nucl. Phys. A* **617** (1997) 472.
- [11] W. Peters, M. Post, H. Lenske, S. Leupold, and U. Mosel, *Nucl. Phys. A* **632** (1998) 109.
- [12] S. Leupold, W. Peters, U. Mosel, *Nucl. Phys. A* **628** (1998) 311.
- [13] L. Tolós, A. Ramos, and A. Polls, *Phys. Rev. C* **65** (2002) 054907.
- [14] L. Tolos, R. Molina, E. Oset and A. Ramos, *Phys. Rev. C* **82** (2010), 045210 (2010).
- [15] G. Agakichiev *et al.* [CERES Collaboration], *Eur. Phys. J. C* **41** (2005) 475.
- [16] J. Seixas *et al.* [NA60 Collaboration], *J. Phys. G* **34** (2007) S1023; S. Damjanovic *et al.*, *Nucl. Phys. A* **783**, 327c (2007); R. Arnaldi *et al.*, *Eur. Phys. J* **C61**, 711 (2009).
- [17] H. van Hees and R. Rapp, *J. Phys. G* **34** (2007) S1051.
- [18] C. Gale and S. Turbide, *Nucl. Phys. A* **783** (2007) 35.
- [19] T. Renk and J. Ruppert, arXiv:hep-ph/0605130.
- [20] E.L. Bratkovskaya, O. Linnyk, and W. Cassing, *Phys. Lett.* **B670** (2009) 428.
- [21] O. Linnyk, W. Cassing, J. Manninen, E. L. Bratkovskaya and C. M. Ko, *Phys. Rev. C* **85** (2012) 024910.
- [22] E. Santini, J. Steinheimer, M. Bleicher, and S. Schramm, *Phys. Rev. C* **84** (2011) 014901.
- [23] H. S. Matis *et al.* [DLS Collaboration], *Nucl. Phys. A* **583** (1995) 617C.
- [24] W. K. Wilson *et al.* [DLS Collaboration], *Phys. Rev. C* **57** (1998) 1865.
- [25] W. K. Wilson *et al.* [DLS Collaboration], *Phys. Lett. B* **316** (1993) 245.
- [26] R. J. Porter *et al.* [DLS Collaboration], *Phys. Rev. Lett.* **79** (1997) 1229.
- [27] G. Wolf, W. Cassing and U. Mosel, *Prog. Part. Nucl. Phys.* **30** (1993) 273; *Nucl. Phys. A* **552** (1993) 549; *Nucl. Phys. A* **545** (1992) 139C.
- [28] E. L. Bratkovskaya, W. Cassing and U. Mosel, *Phys. Lett. B* **376** (1996) 12.
- [29] L. Xiong, Z. G. Wu, C. M. Ko and J. Q. Wu, *Nucl. Phys. A* **512** (1990) 772.
- [30] C. Ernst, S. A. Bass, M. Belkacem, H. Stoecker and W. Greiner, *Phys. Rev. C* **58** (1998) 447.
- [31] E. L. Bratkovskaya, W. Cassing, R. Rapp, and J. Wambach, *Nucl. Phys. A* **634** (1998) 168.
- [32] C. Fuchs, A. Faessler, D. Cozma, B. V. Martemyanov and M. I. Krivoruchenko, *Nucl. Phys. A* **755** (2005) 499.
- [33] E. L. Bratkovskaya and C. M. Ko, *Phys. Lett. B* **445** (1999) 265.
- [34] G. Agakishiev *et al.* [HADES Collaboration], *Phys. Lett. B* **663** (2008) 43 [arXiv:0711.4281 [nucl-ex]].
- [35] Y. C. Pachmayer *et al.* [HADES Collaboration], *J. Phys. G* **35** (2008) 104159.
- [36] M. Sudol *et al.* [HADES Collaboration], *Eur. Phys. J. C* **62** (2009) 81.
- [37] G. Agakishiev *et al.* [HADES Collaboration], *Phys. Lett. B* **690** (2010) 118 [arXiv:0910.5875 [nucl-ex]].
- [38] K. Lapidus *et al.* [HADES Collaboration], arXiv:0904.1128 [nucl-ex].
- [39] G. Agakishiev *et al.* [HADES Collaboration], *Phys. Rev. C* **84** (2011) 014902.
- [40] E. L. Bratkovskaya and W. Cassing, *Nucl. Phys. A* **807** (2008) 214.
- [41] L. P. Kaptari and B. Kämpfer, *Nucl. Phys. A* **764** (2006) 338.
- [42] M. Schäfer, T. S. Biro, W. Cassing and U. Mosel, *Phys. Lett. B* **221** (1989) 1.
- [43] R. Shyam and U. Mosel, *Phys. Rev. C* **67** (2003) 065202.
- [44] F. de Jong and U. Mosel, *Phys. Lett. B* **392** (1997) 273.
- [45] M. Thomere, C. Hartnack, G. Wolf and J. Aichelin, *Phys. Rev. C* **75** (2007) 064902.
- [46] H. W. Barz, B. Kämpfer, G. Wolf and M. Zetenyi, arXiv:0910.1541 [nucl-th].
- [47] E. L. Bratkovskaya and W. Cassing, *Nucl. Phys. A* **619** (1997) 413.
- [48] W. Cassing and E. L. Bratkovskaya, *Phys. Rept.* **308** (1999) 65.
- [49] W. Ehehalt and W. Cassing, *Nucl. Phys. A* **602** (1996) 449.
- [50] K. Weber, B. Blaettel, W. Cassing, H. C. Doenges, V. Koch, A. Lang and U. Mosel, *Nucl. Phys. A* **539** (1992) 713.
- [51] B. Andersson, G. Gustafson and H. Pi, *Z. Phys. C* **57** (1993) 485.
- [52] E. L. Bratkovskaya, W. Cassing and U. Mosel, *Nucl. Phys. A* **686** (2001) 568.
- [53] W. Cassing and S. Juchem, *Nucl. Phys. A* **665** (2000) 377; *ibid.* **A 672**(2000) 417.
- [54] W. Cassing, V. Metag, U. Mosel, and K. Niita, *Phys. Reports* **188** (1990) 363.
- [55] G. Agakishiev *et al.*, [HADES Collaboration], *Eur. Phys. J* **A48** (2012) 64.
- [56] H. Calén *et al.*, *Phys. Rev. C* **58** (1998) 2667.
- [57] P. Moskal *et al.*, *Prog. Part. Nucl. Phys.* **49** (2002) 1.
- [58] P. Moskal *et al.*, *Int. J. Mod. Phys. A* **20**(2005) 1880.
- [59] G. Agakishiev *et al.*, [HADES Collaboration], *Eur. Phys. J* **A48** (2012),74 arXiv:1203.1333 [nucl-ex]

- [60] G. Agakishiev *et al.*, [HADES Collaboration], Phys. Rev. **C85** (2012), 054005 arXiv:1203.2549 [nucl-ex]
- [61] Landolt-Börnstein, New Series, ed. H. Schopper, I/12 (1988).
- [62] F. Balestra *et al.*, Phys. Rev. C **63** (2001) 024004; Phys. Rev. Lett. **89** (2002) 092001.
- [63] S. Teis, W. Cassing, M. Effenberger, A. Hombach, U. Mosel, and Gy. Wolf, Z. Phys. A **356** (1997) 421; Z. Phys. A **359** (1997) 297.
- [64] P. Adlarson *et al.* [WASA-at-COSY Collaboration], Phys. Lett. B **706** (2012) 256 [arXiv:1107.0879 [hep-ex]].
- [65] L. Alvarez-Ruso, E. Oset and E. Hernandez, Nucl. Phys. A **633** (1998) 519 [nucl-th/9706046].
- [66] E. Oset, J. A. Gomez Tejedor, F. Cano, J. C. Nacher, S. Kamalov, L. Alvarez-Ruso and E. Hernandez, Few Body Syst. Suppl. **11** (1999) 275 [nucl-th/9806090].
- [67] X. Cao, B. -S. Zou and H. -S. Xu, Phys. Rev. C **81** (2010) 065201 [arXiv:1004.0140 [nucl-th]].
- [68] O. Buss, T. Gaitanos, K. Gallmeister, H. van Hees, M. Kaskulov, O. Lalakulich, A. B. Larionov and T. Leitner *et al.*, Phys. Rept. **512** (2012) 1 [arXiv:1106.1344 [hep-ph]].
- [69] S.A. Bass *et al.*, Prog. Part. Nucl. Phys. **42** (1998) 279.
- [70] M. Bleicher *et al.*, J. Phys. **G 25** (1999) 1859.
- [71] C. Hartnack, R. K. Puri, J. Aichelin, J. Konopka, S. A. Bass, H. Stoecker and W. Greiner, Eur. Phys. J. A **1** (1998) 151.
- [72] C. Hartnack, H. Oeschler, Y. Leifels, E. L. Bratkovskaya and J. Aichelin, Phys. Rept. **510** (2012) 119.
- [73] J. W. Harris, G. Odyniec, H. G. Pugh, L. S. Schroeder, M. L. Tincknell, W. Rauch, R. Stock and R. Bock *et al.*, Phys. Rev. Lett. **58** (1987) 463.
- [74] W. Reisdorf and Y. Leifels, private communication.
- [75] W. Reisdorf *et al.* [FOPI Collaboration], Nucl. Phys. A **781** (2007) 459 [nucl-ex/0610025].
- [76] M. Antinucci *et al.*, Lett. al Nuovo Cimento, **6** (1973) 121; M. Gaździcki and D. Röhrich, Z. Phys. C **71** (1996) 55; J. Bächler *et al.* (NA49 Collab.), Nucl. Phys. A **661** (1999) 45.
- [77] M. Weber *et al.*, [HADES Collaboration], J. Phys.: Conf. Ser. **316** (2011) 012007.
- [78] M. Lacombe *et al.*, Phys. Lett. B **101** (1981) 139.
- [79] P. Danielewicz and G.F. Bertsch, Nucl. Phys. A **533** (1991) 712.
- [80] J. Weil, H. van Hees, and U. Mosel, Eur. J. Phys. **A 48** (2012) 111.
- [81] D. Schumacher, S. Vogel and M. Bleicher, Acta Phys. Hung. A **27** (2006) 451.
- [82] S. Endres, M. Bleicher, S. Vogel *et al.*, work in progress.
- [83] G. Agakishiev *et al.* [HADES Collaboration], Eur. Phys. J. A **40** (2009) 45 [arXiv:0902.4377 [nucl-ex]].
- [84] S. A. Bass, M. Hofmann, C. Hartnack, H. Stoecker and W. Greiner, Phys. Lett. B **335** (1994) 289.
- [85] The HADES Collaboration web-cite: <http://www-hades.gsi.de/>